J. Indian Inst. Sci., May–June 2000, **80**, 273–306.

IISc THESES ABSTRACTS

Thesis Abstract (Ph.D.)

Fluorine in crystal engineering: Photobehaviour and structure–reactivity correlations of olefins in the crystalline state by K Vishnumurthy
Research supervisor: Prof. T. N. Guru Row
Department: Organic Chemistry

1. Introduction

The advances made in the field of X-ray crystallography and the establishment of the symbiotic relationship between structures and chemical reactivity have paved the pathway for the understanding of reaction mechanisms in the crystalline state. Of special significance is the 2 + 2 photodimerization reaction where the distance between the nearest reactive double bonds is less than 4.2 Å. The additional features are that the double bonds must be nearly parallel and that the stereochemistry of the dimer can be reduced from the contact geometry on the mutual orientation of the reactant molecules. Such reactions are termed topochemically controlled and the main aim of this work is to investigate the part played by fluorine atom in guiding reactant molecules in the crystalline lattice. It is also intended to bring forth the importance of weak and cooperative interactions involving organic fluorine.

2. Solid-state photodimerization reactions: A brief review

The strategies by which the desired molecular packing is achieved in bimolecular photodimerization reactions and the general principles outlining the semantics in crystal engineering are provided with special emphasis on steering capabilities of halogens, methylenedioxy-,

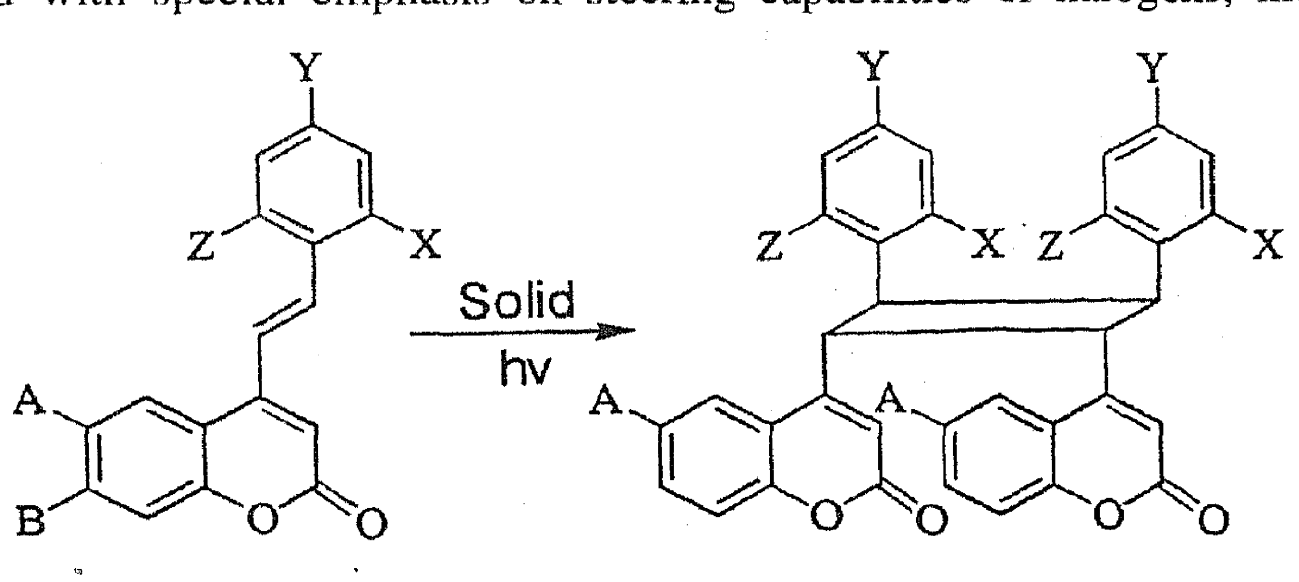

Monofluoro derivatives

1) X = F; Y = Z = A = B = H
2) Y = F; X = Z = A = B = H

Difluoro derivatives

3) A = Y = F; X = Z = B = H
4) A = X = F; Y = Z = B = H
5) X = Z = F; A = B = Y = H

Trifluoro derivatives

6) A = X = Z = F; Y = B = H
7) B = Z = X = F; Z = Y = H
No reaction

methoxy- and acetoxy-induced reactions at defect sites, mixed crystal formation, complex formation with Lewis acids and in host-guest complexes.[1, 2]

3. Structure–reactivity correlations of fluoro-substituted 4-styrylcoumarins in the crystalline state: The β structures[3]

The changes brought about in the packing modes in the crystal lattices by fluorine substitution as compared to those of the parent 4-styrylcoumarin and substituted (other than fluorine) 4-styrylcoumarins are analyzed.[4] However, [2 + 2] photodimerization has been observed specifically across the styrenic double bond. The stereochemistry of the photodimer *syn*-HH (β-packing mode) has been established by single crystal X-ray studies with two examples. This is in contrast to the formation of *anti*-HT, α-packing mode) in the crystals of the 4-styrylcoumarin.[3] The role of intermolecular short contacts C-H...F-C, C-H...O and F...F is discussed.

4. Structure–reactivity correlations of fluoro-substituted 4-styrylcoumarins in the crystalline state: The α structures[5]

The crystal and molecular structures of that fluoro-substituted 4-styrylcoumarins which yield *anti*-HT dimers upon irradiation are described in the crystalline state. A rationale for the lower dimer conversion in 4-styryl-6-fluorocoumarin in terms of involvement of only molecule **B** in photodimerization upon irradiation is suggested. The photo inertness of 4-styryl-7-fluorocoumarin is understood based on geometrical parameters θ_1, θ_2, θ_3 and d which quantify the extent of overlap of the orbitals of the reactive centers. The C=O...Π (phenyl) contacts responsible for the observed *anti*-HT photodimers in 4-(3-fluorostyryl)coumarin and 4-styryl-6-fluorocoumarin are also discussed.

5. Photobehaviour of 7-fluoro-4-methylcoumarin and 6-fluoro-4-methylcoumarin in the crystalline state[6]

The photobehaviour and crystal packing for 7-fluoro-4-methylcoumarin **1** and 6-fluoro-4-methylcoumarin **2** are presented. The anticipated dimer based on studies[3] suggests *syn*-HH,

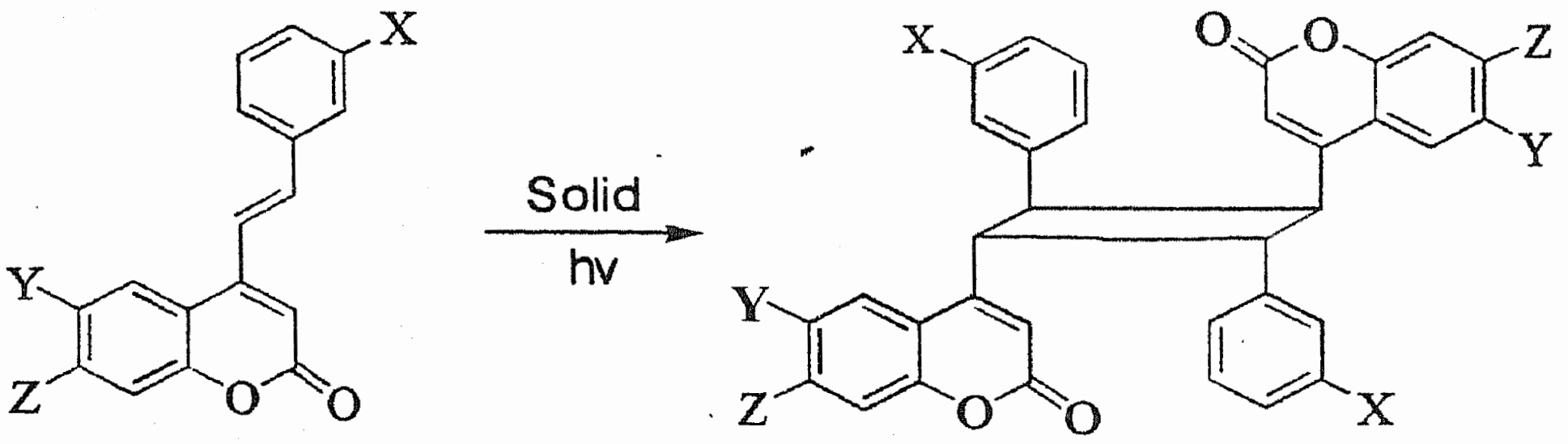

1) X = F; Y = Z = H
2) Y = F; X = Z = H
3) Z = F; X = Y = H ⟶ No Reaction

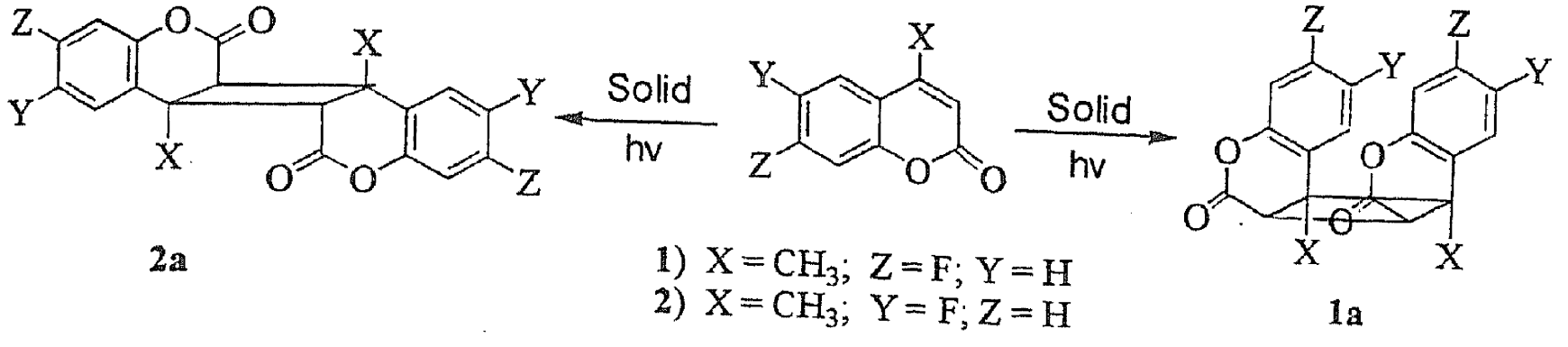

but the crystals of **1** give an *anti*-HT photodimer. On the other hand, crystals of **2** which are expected to yield anti-HT from the packing considerations, produce *syn*-HH dimer. The rationale for such behaviour in the latter is explained in terms of reactions induced at crystal defect sites.

6. Topochemistry of fluoro-substituted (1E, 3E) 1,4-diaryl-1,3-butadienes in the crystalline state: Double [2 + 2] photodimerization

Double [2 + 2] photodimerization of fluoro-substituted (1E, 3E) 1,4-diphenyl-1,3-butadienes is studied to investigate the effective dimerization across both the double bonds. Fluoro substitution reorganizes the molecules favouring photoreaction. Based on the single-crystal X-ray studies of the monomers, the observed crystal packing corresponds to α-packing mode. The lower dimer conversion, ~25%, in all the cases is rationalized. Based on the molecular organization, it is observed that in the centrosymmetric molecular alignment in the reactants, C-H...F-C and F...F contacts seem to provide additional supportive interactions.

7. Generation of polymorphic forms in 4-styrylcoumarins using coumarin as an additive: Impact on photodimerization reactions

The polymorphic of parent 4-styryl coumarin[4a] and 4-(3-fluorostyryl) coumarin obtained with the addition of coumarin (2.5% by molar ratio) during crystallization has been studied via X-ray diffraction. The structures, crystal packing and the photobehaviour have been examined.

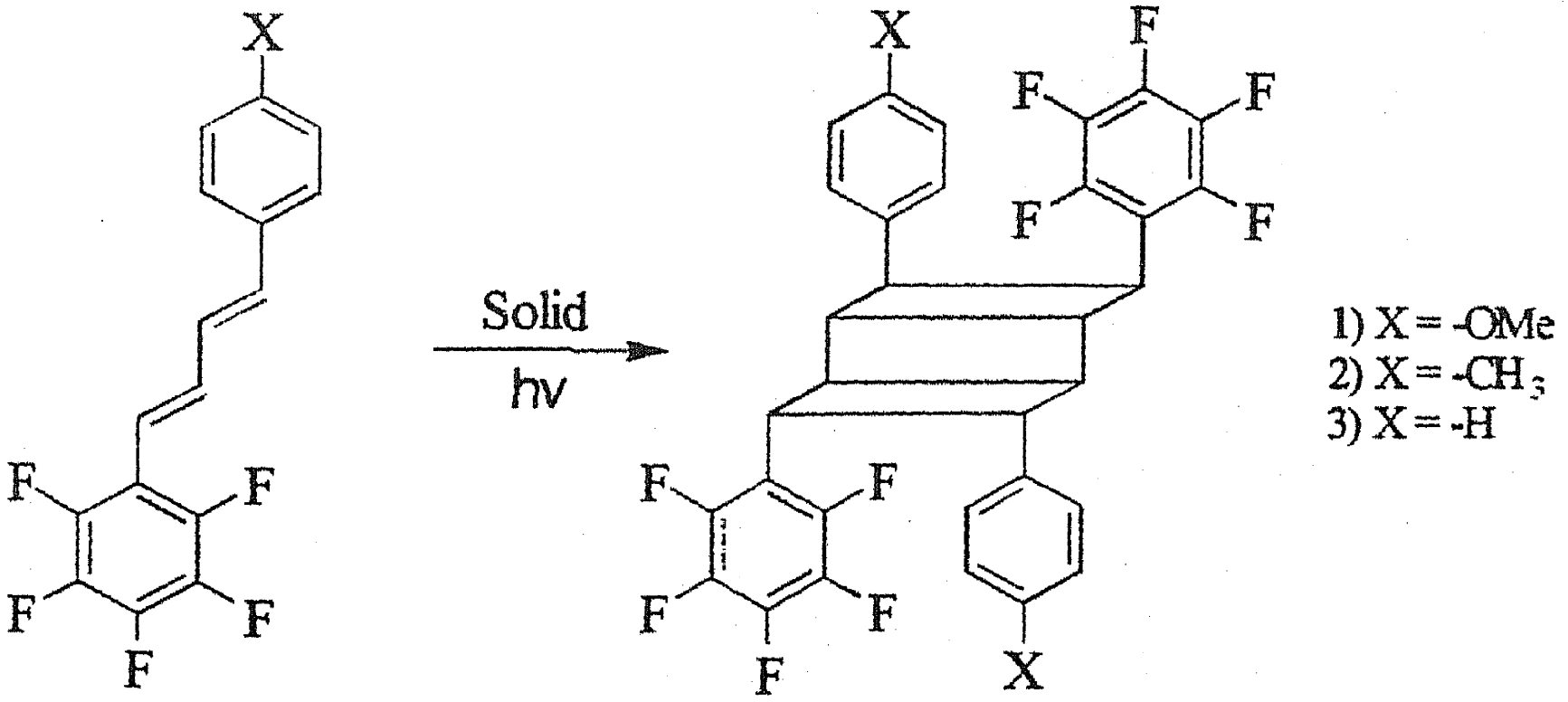

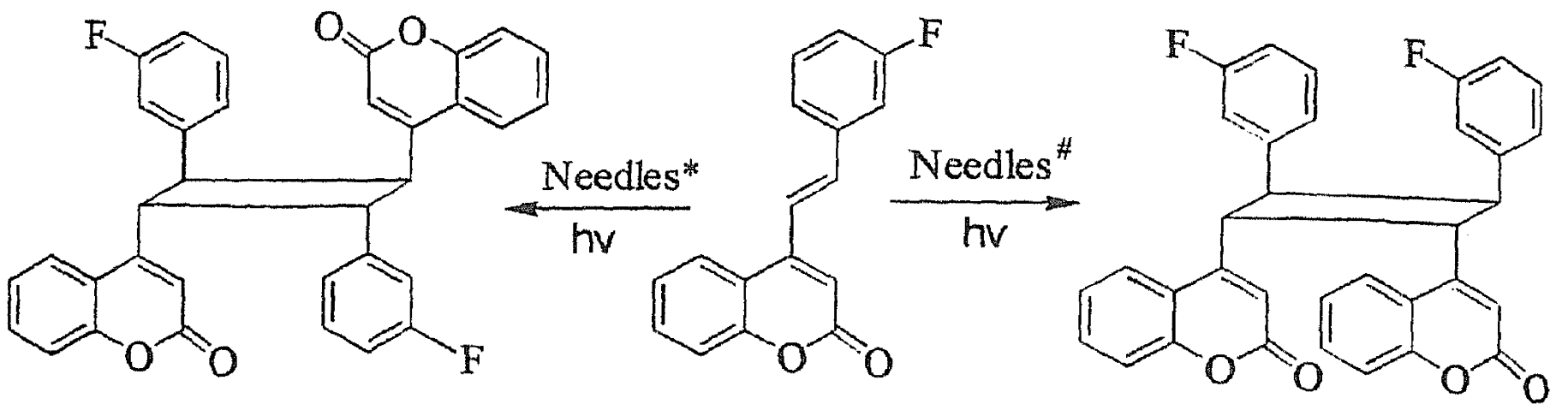

*Crystals obtained without the addition of coumarin during crystallization.
#Crystal obtained by adding coumarin as an additive during crystallization.

The author also demonstrates the use of coumarin as an additive to generate X-ray-quality crystals in (1E, 3E) 1,4-diphenyl-1,3-butadiene.

References

1. RAMAMURTHY, V. AND VENKATESAN, K. *Chem. Rev.*, 1987, **87**, 433–481.
2. VENKATESAN, K. AND RAMAMURTHY, V. *Photochemistry in organized and constrained media* (Ramamurthy, V. ed.), Ch. 4, VCH, 1991, 133–161.
3. VISHNUMURTHY, K., GURU ROW, T. N. AND VENKATESAN, K. *J. Chem. Soc., Perkin Trans.* 2, 1996, 1475–1478.
4(a) NARASIMHA MOORTHY, J. AND VENKATESAN, K. *Bull. Chem. Soc. Jap.*, 1994, **67**, 1–6.
4(b) NARASIMHA MOORTHY, J., SAMANT, S. D. AND VENKATESAN, K. *J. Chem. Soc., Perkin Trans.* 2, 1994, 1223–1228.
5. VISHNUMURTHY, K., GURU ROW, T. N. AND VENKATESAN, K. *J. Chem. Soc., Perkin Trans.* 2, 1997, 615–619.
6. VISHNUMURTHY, K., GURU ROW, T. N. AND VENKATESAN, K. *Tetrahedron*, 1998, **54**, 11235–11246.

Thesis Abstract (M.Sc. (Engng))

Determination of phase diagrams of model alloy systems – A Monte Carlo study by H. Ramanarayan
Research supervisor: Dr T. A. Abinandanan
Department: Metallurgy

1. Introduction

We have used a novel Monte Carlo algorithm, proposed recently by Lee,[1] for determining the phase diagrams of two model alloy systems. Lee's algorithm was chosen because of its generality and for its ability to directly yield the density of states $\Omega(c, E)$ and hence the entropy $S(c, E)(= \log(\Omega(c, E))$, of the system in one simulation. Since $S(c, E)$, the entropy expressed as a function of the alloy composition (c), and energy (E) is a fundamental thermodynamic relation, all other thermodynamic information can be obtained from it. We have studied the progress of the simulations to arrive at criteria for deciding when the simulations must end. We

have also critically examined the quality of the $S(c, E)$ data obtained from the simulations by comparing them with known exact results for a set of carefully selected atomic configurations in systems with a few atoms in the binary alloy.

We have studied two model alloy systems based on the square lattice of size $L \times L$; the first is a simple phase separating system with nearest neighbour interatomic interactions extending up to the second neighbour shell. The former is the alloy of the ferromagnetic Ising model and has an exact solution. The latter has a tricritical point in the phase diagram.

2. Spinodal decomposition

The simulation of the phase-separating system gave us an opportunity to compare our result with the already available exact solution by Onsagar.[2] It also enabled us to address the controversy present in the literature regarding the existence of spinodal point in the thermodynamic limit. For the phase-separating system with a positive value of $W_{AB}^{(i)}$ defined by,

$$W_{A,B}^{(i)} = \frac{1}{4}\left(2E_{A,B}^{(i)} - E_{A,A}^{(i)} - E_{B,B}^{(i)}\right),$$

where $E_{X,Y}^{(i)}$ is the bond energy between X and Y species in the ith neighbour shell of each other. The free energy vs composition (G *vs* c) curves for finite sizes are U shaped at high temperatures and W shaped at low temperatures, indicating complete solid solubility at high temperatures and two-phase coexistence at low temperatures. We studied the behaviour of G *vs* c curves at low temperatures for various system sizes ranging from $L = 10$ to 20. We find that the difference between the minimum free energy values at the two-phase coexistence compositions and that at composition $c = 0.5$ decreases as the lattice size increases. This indicates strongly that at infinite size, the system, devoid of finite size effects, will have a G *vs* c curve with two-phase region represented by the common tangent to the single phase region. This leads to the conclusion that the spinodal point does not have a thermodynamic validity, supporting the results of previous work done in this area. For $W_{AB}^{(1)} = 1$ and a lattice size of $L = 20$, our best estimates for the compositions of the two coexisting phases are 0.0475 and 0.9525 at a temperature of $\frac{K_B T}{W_{AB}^{(1)}} = 2.1$ and their free energy is –2.05015. In comparison, the exact solution yields 0.0656, 0.9344, and –2.0688, respectively. Similarly, the critical point (the highest temperature of two-phase coexistence) for $L = 20$ is estimated to occur at $\frac{K_B T}{W_{AB}^{(1)}} = 2.2890$ while the exact solution yields 2.2692.

3. Ordering system

The second model alloy system in characterized by ordering energies $W_{AB}^{(1)} = -1$ and $W_{AB}^{(2)} = 1/2$ for the first two neighbour shells; these values stabilize two terminals solid solutions and an ordered phase at the stoichiometric composition of $c = 0.5$ at low temperatures. The phase diagram for this system exhibits a tricritical point, at which a second-order transition (order to disorder) line meets two first-order transition lines (phase boundaries which are the limits of stability of the terminal solid solution and the ordered phase at low temperatures). Our

attempt in the work was to determine the phase diagram of this system and, in particular, locate the position of the tricritical point in the phase diagram. At intermediate temperatures, the ordered alloys of composition near $c = 0.5$ undergo a second-order phase transformation to a disordered state; this transformation is marked by a singularity in specific heat capacity (C_v) at the critical temperature, which for finite systems, is manifested as a peak in the (C_v vs T) curves. This peak position is taken as the critical temperature for finite systems. The locus of the critical temperature for different compositions forms the second-order line. At low temperatures, the phase diagram exhibits a two-phase region in which a terminal solid solution and the ordered phase coexist at equilibrium. The compositions of the two phases are given by the common tangent construction to the G vs c curves. For calculating these compositions, we make use of the grand canonical probability function $P_{(T,\ \Delta\mu)}(c)$ at a constant temperature (T) and difference in chemical potential ($\Delta\mu$). $P_{(T,\ \Delta\mu)}(c)$ exhibits a two-peak structure for certain values of $\Delta\mu$ at a given (low) temperature. The compositions corresponding to the two peaks when they have the same height (which occur for a critical value of $\Delta\mu$) are taken as the compositions of the two phases. From the second- and first-order lines obtained as above, the phase diagram with the tricritical point is generated for the ordering system. Our best estimate, for the largest system size of $L = 20$, for the composition (c_t) and scaled temperature $\frac{K_B T}{W_{AB}^{(1)}}$ at the tricritical point are 0.26 and 1.62, respectively. Similarly, our best estimate of the scaled critical temperature $\frac{K_B T}{W_{AB}^{(1)}}$ is 3.8 for a composition $c = 0.5$. Our work has established the efficacy of the Lee algorithm for phase diagram calculation in finite, but small, systems; the data obtained in this study, however, appear to be insufficient for undertaking a detailed finite size scaling analysis for extrapolating to infinite (thermodynamic) systems.

References

1. LEE, J. — *Phys. Rev. Lett.*, 1993, **71**, 211.
2. ONSAGAR, L. — *Phys. Rev. Lett.*, 1944, **65**, 117.
3. BINDER, K. — *Spinodal decomposition*, Vol. 5, *Materials Science and Technology, Phase Transformations in Materials* (Hassen, P. ed.), VCH Publishers, 1990.
4. LAUGHLIN, D. E. AND SOFFA, W. A. — Exosolution, ordering and structural transformations: systematics and synergitics, in *Physical properties and thermodynamic behaviour of minerals* (Salje, E. K. H. ed.), NATO ASI Series, C, 1988, Vol. 225, p. 213.

Thesis Abstract (Ph.D.)

Structural characterization of protein folding intermediates by Surajit Bhattacharjya
Research supervisors: Profs P. Balaram and Anil Kumar
Department: Molecular Biophysics Unit

1. Introduction

The ability of a newly synthesized polypeptide chain to fold rapidly and efficiently into its highly specific three-dimensional structure is an essential part of the conversion of genetic in-

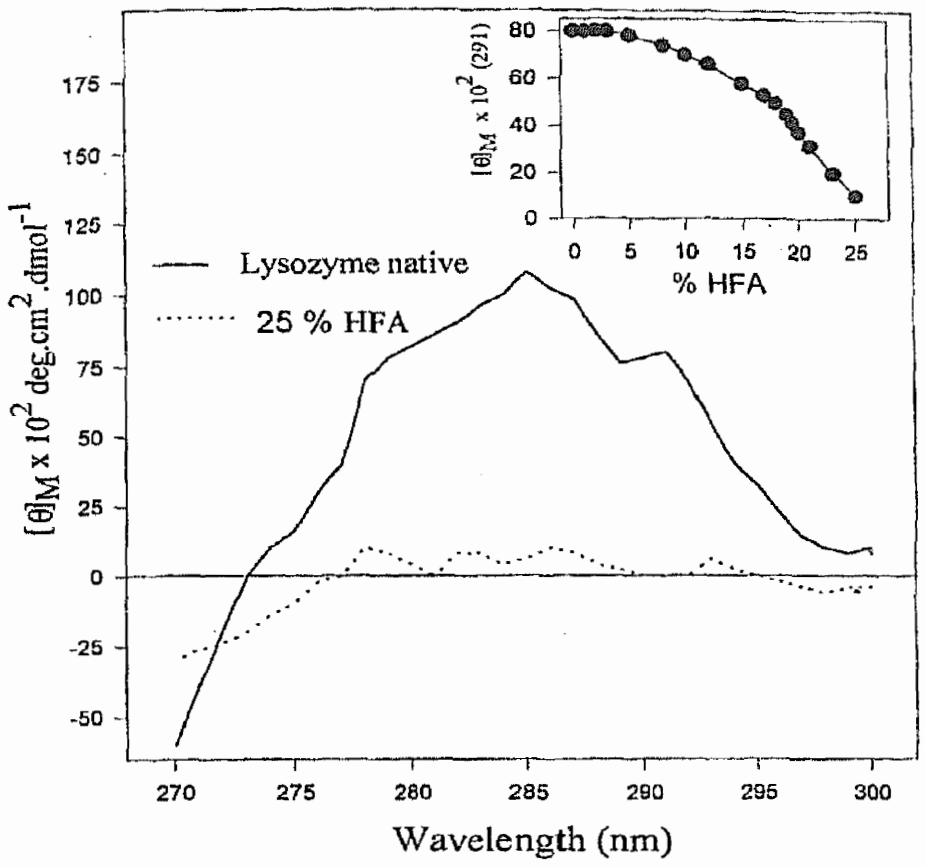

FIG. 1. Near-UV CD spectra of lysozyme in native state in aqueous solution and in 25% HFA. **Inset**: Dependence of near-UV CD ellipticity at 291 nm of HFA concentration.

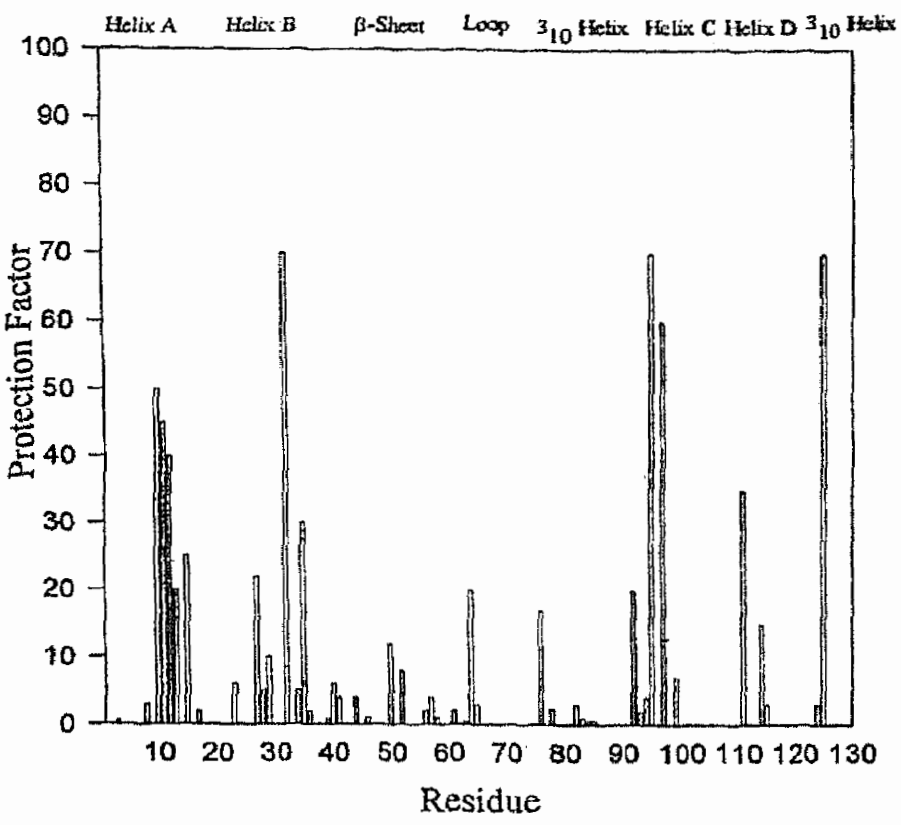

FIG. 2. Bar diagram showing distribution of protection factors of the amide protons of lysozyme in 25% HFA. Regions of secondary structure in the native state are marked at the top.

formation into cellular activity. In contrast to our present knowledge of the major cellular processes like transcription, replication or translation, comparatively little is understood how

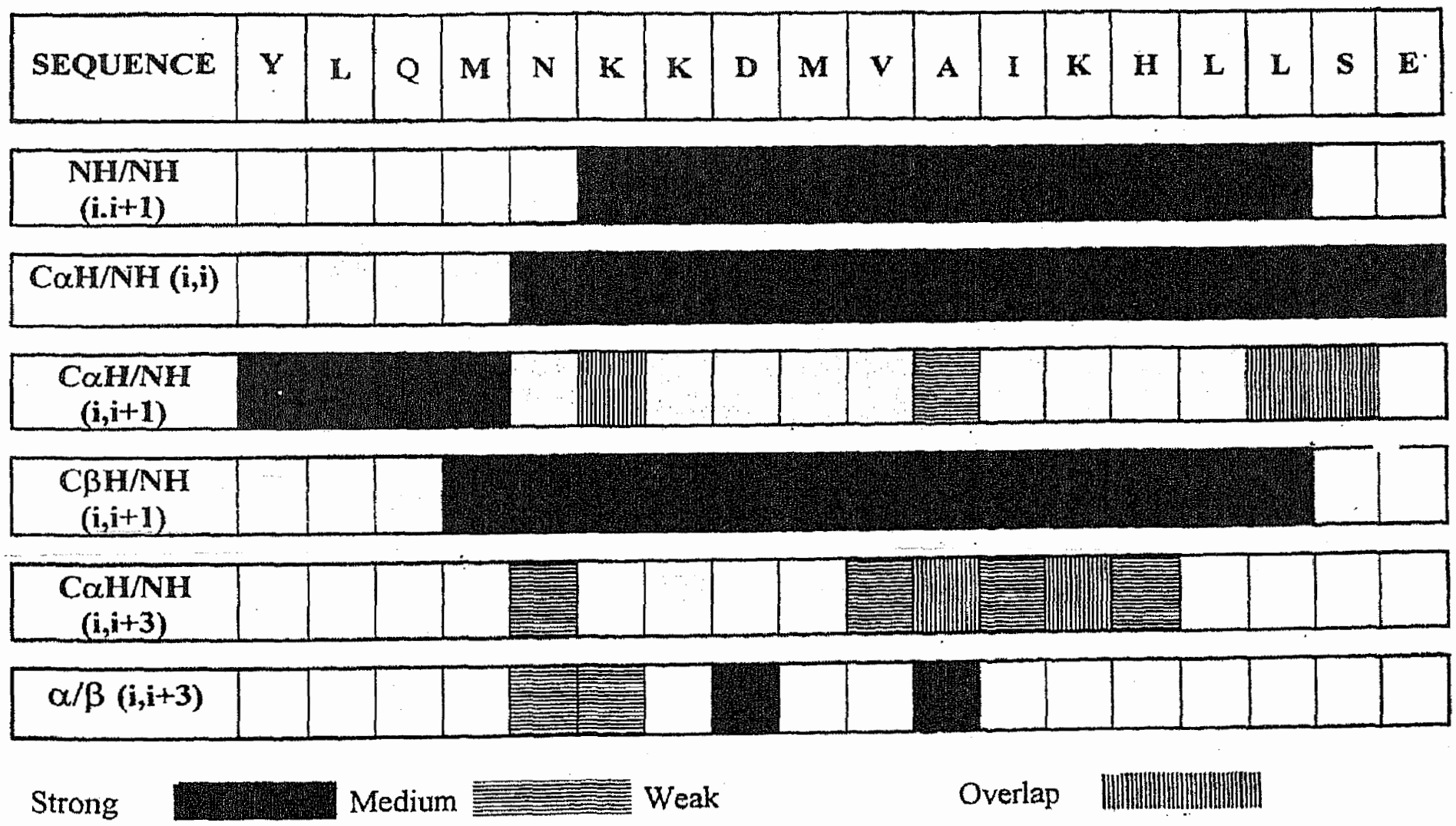

FIG. 3. NOE summary for peptide R18 in 50% HFA. The amino-acid sequence is shown at the top. The intensities of the NOEs are categorized as either strong, medium or weak and marked accordingly by different shades.

this occurs. It was pointed out by Anfinsen in the late 1950s, that all the information needed to obtain the three-dimensional fold of a protein is encoded into its one-dimensional amino-acid sequence.[1, 2] The mechanism by which this process takes place is a central issue in structural biology. Proteins do not fold by a random, unbiased search of all the conformational space as this would require enormous time scale for folding. This has led to the idea that there must be a defined pathway and limited intermediates in folding.[3] Therefore, the study of folding intermediates should provide valuable insights into protein folding process. Here, we describe structural characterization of intermediate states of hen lysozyme, riboflavin carrier protein (RCP) and thymidylate synthase (TS). Two partially unfolded states of lysozyme have been characterized in 50% DMSO and 25% HFA. Synthetic peptide fragments from RCP and TS have been studied to investigate early events in the protein-folding process.

2. Results and discussion

A molten globule-like intermediate state of lysozyme has been characterized in 25% HFA by CD, fluorescence, NMR and H/D exchange. This intermediate state has the following structural features: (a) Persistent native-like secondary structures and loss of tertiary structures as evident from CD experiments (Fig. 1). (b) Strong interaction with the hydrophobic dye ANS. (c) Absence of the 'ring current' affected ^{1}H resonances in NMR experiments indicating disruption of the native fold. (d) Solvent inaccessibility of the tryptophan residues, as judged

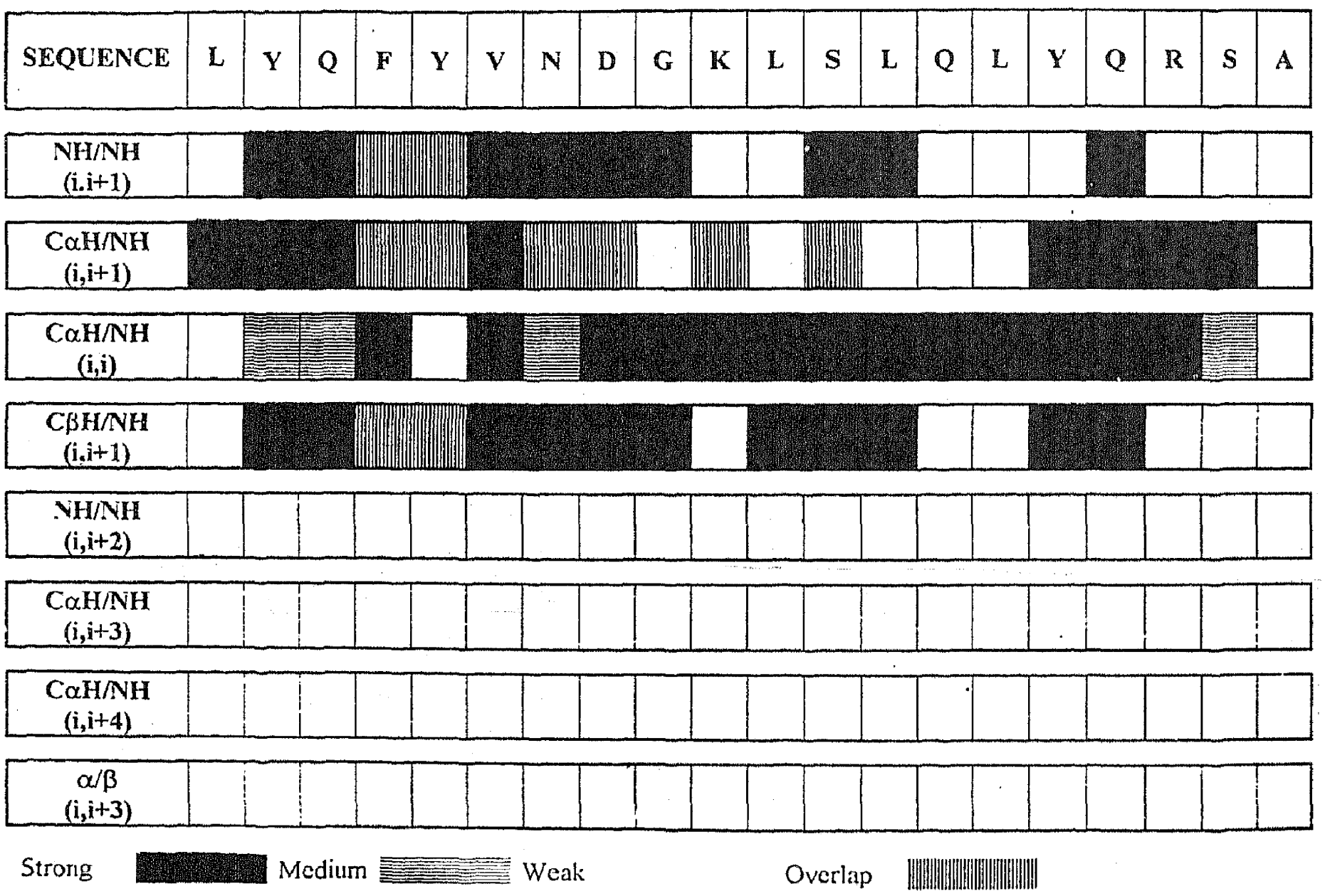

FIG. 4. NOE summary for peptide C20 in 50% HFA. The amino-acid sequence is shown at the top. The intensities of the NOEs are categorized as either strong, medium or weak and marked accordingly by different shades.

by fluorescence quenching and H/D exchange suggestive of a compact structure. (e) A cooperative thermal unfolding of the intermediate state to a further unfolded state supports the existence of side chain interactions in stabilizing the compact structure. (f) Protection factor analysis from H/D exchange experiments clearly suggests a 'bipartite structure' of the intermediate state,[4] where helical structures are largely retained with preferential loss of β-sheet structures (Fig. 2). The structural characteristics of the intermediate state of lysozyme in 25% HFA are quite similar to the molten globule-like states of many proteins, including the structurally homologous protein α-lactalbumin. On the other hand, a highly ordered molten globule-like state of lysozyme is formed in 50% DMSO. This state has high near-UV CD and higher protection factors. This state of lysozyme is similar to the Ca^{+2}-depleted state of equine lysozyme.[5] These results indicate that a large repertoire of organic solvents with contrasting physical properties will certainly be of great advantage in stabilizing a wide range of intermediate states of proteins.

Three synthetic antigenic peptides from RCP corresponding to residues 4-23 (N21), 170-186 (R18) and 200-219 (Y21) have been examined in water and in water/50% HFA. All the peptides are unstructured in aqueous solution; however, a dramatic stabilization of helical structure has been observed for the R18 and Y21 peptides in 50% HFA as suggested by CD spectra and NOEs (Fig. 3). However, no stable structures have been detected for the N21 peptide even at higher concentrations of HFA. The Y21 and R18 peptides form a helical conformation in the crystal structure of RCP, whereas N21 is in an extended conformation. Three synthetic peptide fragments comprising the residues, 17-38 (N22), 174-190 (M17) and 201-220 (C20), from the dimer interface of TS have been studied. NMR studies show a nascent helical conformation for the C20 peptide; the helical structure is largely stabilized in 50% HFA (Fig. 4). Interestingly, this peptide fragment is in a β-hairpin conformation in the native structure of TS. The N22 and M17 peptides form native-like β-strands in a 50% HFA/water mix-

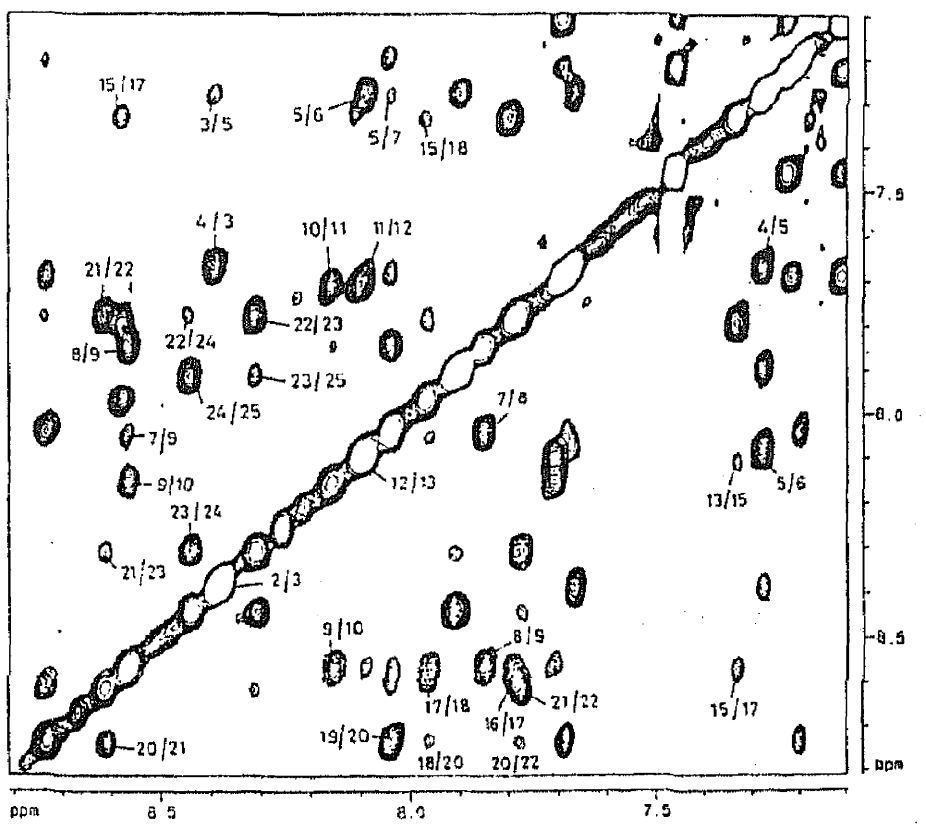

FIG. 5. Partial NOESY spectrum of melittin in 50% HFA, pH 2.0 showing NH/NH NOE connectivities. A mixing time of 300 ms was used for the NOESY experiments.

ture. A population of non-native β-turn conformations has been detected for the M17 peptide at the C-terminus.

In order to stabilize a native-like β-hairpin conformation in the C20 peptide, a D-Pro residue has been introduced in place of Asp8. D-Pro has been successfully used in *de novo* design strategies directed towards the construction of β-hairpins.[6, 7] The results suggest that even in the D-Pro analog the extent of β-hairpin formation is relatively low in aqueous solution. Surprisingly, the addition of structure-stabilizing cosolvents results in a shifting of the conformational equilibrium towards helix formation in short segments flanking the D-Pro residue. It is clear from these results that although the 201-220 segment TS adopts a β-hairpin structure in the native protein, this conformation is not favoured in the synthetic fragment.

The ability of HFA to stabilize helical structures has been investigated in melittin, a peptide from honey bee venom. The conformation of melittin is largely unstructured at low pH due to unfavourable charge/charge repulsion at the C-terminus. A helical structure of melittin at low pH in 50% HFA is established by CD and NMR. A sharp transition from a random coil conformation to a largely helical conformation, on titrating an aqueous solution of melittin with HFA has been observed. This transition is completed by 50% HFA. Figure 5 shows diagnostic NH/NH NOEs suggesting a helical conformation of melittin at 50% HFA, pH 2.0.

References

1. ANFINEN, C. B., HABER, E., SELA, M. AND WHITE, F. M. — *Proc. Natn. Acad. Sci. USA*, 1961, **47**, 1309–1314.
2. HABER, E. AND ANFINSEN, C. B. — *J. Biol. Chem.*, 1962, **237**, 1839–1844.
3. LEVINTHAL, C. — *Mossbauer spectroscopy in biological systems*. Proceedings of a meeting held at Allerton house, Monticello, Illinois (P. Debrunner, J. Tsibris and E. Munck, eds), 1969, pp. 22–14 (University of Illinois Press, Urbana, Illinois).
4. PENG, Z. AND KIM, P. S. — *Biochemistry*, 1994, **33**, 2136–2141.
5. MOROZOVA, L. *et al.* — *Nature Struct. Biol.*, 1995, **2**, 871–875.
6. KARLE, I. L., AWASTHI, S. K. AND BALARAM, P. — *Proc. Natn. Acad. Sci. USA*, 1996, **93**, 8189–8193.
7. HAQUE, T. S., LITTLE, J. C. AND GELLMAN, S. H. — *J. Am. Chem. Soc.*, 1996, **118**, 6975–6985.

Thesis Abstract (Ph.D.)

Community ecology of small mammals in montane ecosystems of the Nilgiris, southern India by Kartik Shanker
Research supervisor: Prof. R. Sukumar
Department: Centre for Ecological Sciences

1. Introduction

The study of the distribution and diversity of plants and animals has acquired much importance in recent years. The theory of island biogeography of MacArthur and Wilson[1] has been ex-

tended to fragmented and isolated patches of forests on land and the island metaphor has taken on greater importance in the context of the design of nature reserves for conservation. Another key issue in community ecology is interspecific competition, whose importance in structuring small mammal communities is still unclear, especially in tropical forests.[2, 3] The demography of insular populations of small mammals has also been of interest.[4] This study deals with the community ecology of small mammals in naturally fragmented forests in the Upper Nilgiris in southern India, focusing on aspects of demography in the context of insularity and the role of habitat selection and interspecific competition in the structuring of these communities.

2. Study area

The natural habitat of the Upper Nilgiris, a part of the Western Ghats range in South India, comprises patches of montane evergreen forest (or *shola*), surrounded by grassland, which provide an ideal 'laboratory' to study the effects of insularity and fragmentation. Further, the *shola* patches have been subjected to disturbance in many areas, many grasslands having been replaced by plantations of tea (*Camellia sinensis*), bluegum (*Eucalyptus globulus*), wattle (*Acacia spp.*) and pine (*Pinus roxburghii*). The *shola* patches chosen for the study were primarily in the relatively undisturbed Upper Bhavani region of the Upper Nilgiris. Plantations were sampled at sites adjacent to Upper Bhavani and Thaishola, which at 600 ha, is the largest *shola* patch in the Nilgiris.

3. Methods

Small mammals (rodents and insectivores) were studied using standard Sherman live traps on grids of 0.5 to 1 ha. Eight *shola* patches (0.2 to 600 ha) were sampled from February 1994 to September 1996. Open grasslands and grasslands between patches were also sampled during this period. Tea, wattle, eucalyptus and pine plantations were sampled from February 1995 to November 1995, using rectangular 0.45 ha grids. Removal and introduction experiments were conducted in two small *shola* patches (0.1–0.5 ha). Sampling sessions typically lasted five days from February 1994 to October 1994, and three days thereafter. Each plot was typically sampled once in each season, for a total of ~ 35,000 trap-nights.

4. Results and discussion

A total of 9 species were trapped with an average trapping success of 10.1%, of which there were 8 species in *sholas*, 3 in the grassland, 3 in wattle, eucalyptus, and pine plantations and 4 in tea plantations. *Rattus rattus* was the dominant species in the *shola*, comprising 60.9% of total density, while *Millardia meltada* was the dominant species in the grassland. *Suncus montanus*, a shrew, was the only species captured in both habitats. *Rattus rattus* and *Millardia meltada* coexisted in the plantations. The other common species in the *sholas* included *Mus famulus* and *Suncus dayi*. The largest *shola* patch (600 ha) had 8 species, the intermediate (60 ha) 6 species, while smaller (0.1 to 10 ha) 4 species.

Different aspects of trapping in tropical forests were examined, including the estimation of abundance and species richness for *Rattus rattus*. Estimates were derived from various models used in mark-recapture experiments. In our sample, the precision of the estimators increased

with the duration of sampling and with capture probability; however, the trap mortality also increased with the sampling duration. In smaller patches, 3 days of sampling seemed the optimal trade-off between mortality and precision. Due to low capture probabilities for species other than *Rattus rattus*, and the latter's low sample sizes, it was not possible to use the estimators and models consistently. Hence, the Minimum Number Alive was used as a standard estimate for the entire study. Species richness was higher in some seasons than in others, with new species being trapped even after one year of trapping.

Synchrony in 12 population variables in 8 *shola* patches and two plantations was examined for *Rattus rattus* and other small mammals. Synchrony in *Rattus rattus* age structure was relatively high. Within-site synchrony was higher than between-site synchrony for *Rattus rattus* population variables. The seasonal nature of climate in the area and phenology of the forests may be responsible for synchronous breeding in this species. However, the correlation in *Rattus rattus* density was significantly higher within the single large unfragmented patch than between several small fragmented patches. The removal experiments demonstrated that different patches take different periods of time to recover from depletion and this could lead to asynchrony. Hence, demographic and environmental stochasticity may contribute to fluctuations in small populations, leading to asynchrony even at small spatial scales and the establishment of synchrony may be impeded by poor dispersal across the grasslands.

Densities of small mammals (total–20.6/ha; *Rattus rattus*–13.5/ha) seemed higher than those reported for lower evergreen contiguous forests in southern India. Contrary to expectations, densities were not higher in smaller than in larger patches. Despite this, many of the demographic effects that are characteristic of insular populations were observed in these populations. Proportion of adults was higher in smaller patches, while proportions of juveniles and sub-adults were higher in the large patch. The mean weight of adult males was negatively correlated with patch size. The abundance and biomass of species other than *Rattus rattus* were negatively correlated with canopy height, while the proportion of *Rattus rattus* was positively correlated with canopy height. In general, population characteristics of *Rattus rattus* were related to patch size, while small mammal community structure variables were related to habitat structure. Average species richness was highest in the smaller patches, though this may be due to higher densities of rare species in these patches, which again would be due to the higher diversity of forest floor niches; the rarer species, *Suncus montanus*, *Suncus dayi* and *Mus famulus*, are all forest floor species.

Canonical discriminant analysis was performed to determine if there was habitat selection by the forest species. At the microhabitat level, all three common forest species – *Rattus rattus*, *Mus famulus* and *Suncus montanus* – were found to show habitat discrimination based primarily on tree density. *Mus famulus* used areas of higher tree density than the other two species. Analysis of spatial interactions of these three species revealed neither overlap nor avoidance, implying that densities are so low that the conditions for such interactions may not have arisen.

In the natural habitat (*shola* and grassland), *Rattus rattus* and *Millardia meltada* were mutually exclusive. While the former was trapped in the *shola* forest patches, the latter was the only rodent trapped in the grassland. *Millardia meltada* did not colonise *shola* patches following complete removal of *Rattus rattus* from these patches, nor did they remain and survive in *sholas* when introduced (following *Rattus rattus* removal). Analysis of wattle stands of differ-

ent ages revealed that *Millardia* dominated young stands (grass-like habitat), while *Rattus* dominated the older stands (forest-like habitat). In habitats where they co-occurred, there was no evidence of overlap or avoidance. In old wattle stands, *Millardia* used areas of higher ground cover than did *Rattus*. The available evidence thus suggests that interspecific competition is not an important factor in structuring these communities.

Rattus rattus and *Millaria meltada* reached the highest densities in plantations, the former averaging 16.6 individuals/ha in old wattle plantations and the former averaging 25.5 individuals/ha in middle-aged wattle plantations. The density of *Millardia* in plantations is especially high compared to natural habitats. An examination of the *shola*-plantation edges did not show any differences in density or age structure of *Rattus rattus* between the *shola*, edge and plantation. However, there were apparent differences in age structure of *Rattus rattus* between the *sholas* and the plantations with the old wattle plantations resembling the *sholas* most closely. The extensive spread of the plantations may alter the demography of small mammals in the forests, and of carnivores that depend on these species. Hence, plantations need to be managed with care, since the small mammal communities vary greatly depending on the type of the habitat and its age.

5. Conclusion

In conclusion, it is clear that the demography of these insular small mammal populations is different from those in contiguous forests and this could have important consequences for predators and the dynamics of the system. Lower synchrony in fragmented patches and results from the removal experiments demonstrate that the grasslands constrain dispersal, leading to insularity effects in the demography and community structure of the small mammals in the patches. It also appears that interspecific competition does not play an important role in the structuring of the community. The introduction of plantations to replace grasslands may seriously affect the dynamics of forest populations of small mammals and management policies need to take these factors into consideration.

References

1. MACARTHUR, R. H. AND WILSON, E. O. *The theory of island biogeography*, Princeton University Press, 1967.

2. CONNELL, J. H. On the prevalence and relative importance of interspecific competition: evidence from field experiments, *Am. Naturalist*, 1983, **122**, 661–696.

3. SCHOENER, T. W. Field experiments on interspecific competition, *Am. Naturalist*, 1983, **122**, 240–285.

4. ADLER, G. H. AND LEVINS, R., The island syndrome in rodent populations. *Q. Rev. Biol.*, 1994, **69**, 473–490.

Thesis Abstract (Ph.D.)

Strategies for modulation of allergen-specific immune responses to the major shrimp allergen, tropomyosin by Deepa Rajagopal

Research supervisors: Prof. P. V. Subba Rao and Dr. Apurva Sarin
Department: Biochemistry

1. Introduction

Immune responses are an outcome of the interaction of a network of cells, namely, the T-, B- and antigen-presenting cells. While a fruitful interaction of the components of the immune system helps to counteract diseases and infections, harmful manifestations of the immune responses also do occur. Allergic responses and autoimmune disorders fall under such a category of 'aberrant immune responses'. The patho-physiological outcome of an allergic reaction is mediated by circulating allergen-specific IgE antibodies produced in response to minute doses of allergen.[1, 2]

The role of allergen-specific IgE and mast cells in the etiology of immediate type hypersensitivity has been well established in addition to the involvement of eosinophils, neutrophils and basophils in the late phase reactions associated with atopic disease. The cytokines that influence IgE production,[3] early mediator release and late-phase inflammatory responses have been the focus of intense research. Besides the significance of the central role of allergen recognition, the role and importance of costimulation mediated by cognate interactions and cytokines (which tend to act in a cooperative way) are becoming increasingly clear.[4] The fine regulation of different immune components thus ultimately dictate the functional quality of the ensuing immune responses.

Crustacean food allergy is known to provoke gastrointestinal as well as systemic allergic reaction. Earlier work as described in brief in the thesis leads to the purification of the major cross-reacting crustacean food allergen from shrimp as the heat-stable muscle protein, tropomyosin.[5] From an immunological standpoint, the modulation of allergen-specific immune responses was consequently of interest. The results presented in the work suggest that the definition of immunogenic components involved in an allergic response can help in the development of strategies that can regulate specific effector responses leading to allergy.

The present study thus addresses the possibility of modulation of allergen-specific immune responses contextually to the food allergen, shrimp tropomyosin. The responses to tropomyosin were found to vary with the host genetic background. The cellular proliferative responses to recall with tropomyosin were found to be in concordance with the observed titers of allergen-specific IgG and IgE antibodies. The administration of allergen covalently linked to isologous IgG provides a novel strategy for the conversion of allergens to tolerogens and consequent suppression of antibody responses *in vivo*. Intravenous administration of an isologous IgG conjugate of shrimp tropomyosin was found to induce a reduction in the allergen-specific IgG and IgE responses. The conjugate of 41-mer peptide (29–69), encompassing the previously identified B-cell epitope with isologous IgG, was also found to induce suppression *in vivo*. These studies stress upon the significance of defined allergenic epitopes for tolerance induction, in addition to providing a new strategic approach for regulation of immune responses.

2. Experimental and discussion

The possible potential of peptide epitopes to decrease a specific antibody response to tropomyosin was next investigated. Six peptides predicted based on a computer algorithm to be candi-

date T-cell epitopes were synthesized and purified by HPLC. A 21-mer synthetic peptide was found to induce proliferation comparable to the native allergen and was tested for its ability to modulate allergen-specific humoral immune responses. The peptide when administered either subcutaneously in Freund's adjuvant or as a single dose in the soluble form was found to significantly reduce the ongoing allergen specific IgG and IgE responses. The peptide-treated mice, however, did not show a reduction in the proliferative response to either tropomyosin or the peptide itself indicating that the observed reduction of ongoing humoral responses could be due to an alteration in the cytokine profiles *in vivo*. The modulation by the peptide was found to be haplotype specific. These results are consistent with the conclusion that synthetic peptide is capable of down regulating the sea food allergen specific immune responses *in vivo*.

The role of antigen presenting cells as being capable of modulating the outcome of an immune response and varying in their ability to induce a type I versus a type II response was investigated. Maleylated proteins are known to be specifically targeted to macrophage scavenger receptors. Since macrophages as antigen presenting cells lead to the induction of Th1 responses and allergic responses are characterized by a polarization towards Th2 phenotype, the possibility of modulation by targeting to macrophages was explored. Analysis of cytokine profiles showed a modulation towards a maleylated tropomyosin, induced IFN-gamma dominant, anti-allergic phenotype, which could also be correlated, to the *in vivo* antibody isotype suggesting the possible potential of modulation of allergic responses *in vivo*.

Chemically modified allergens or allergoids have been explored for their use as an alternative to native allergen immunotherapy. Such a hypoallergenic variant with a diminished ability to bind allergen-specific IgE in addition to enhanced cellular proliferation, was able to mediate a specific down regulation of humoral responses to shrimp tropomyosin.

All these factors therefore have an impact on the outcome of a response, the knowledge of which is important for effective immunization strategies. Since a multitude of factors lead to the initiation of a response to a protein antigen, the strategies for modulation also need to be multi factorial requiring a complete understanding of the underlying regulatory mechanisms.

References

1. JAN DE VRIES — Atopic allergy and other hypersensitivities, *Curr. Opin. Immunol.* 1994, **6**, 835.
2. ISHIZAKA, K. — Basic mechanism of IgE mediated hypersensitivity, *Curr. Opin. Immunol.*, 1989, **4**, 625.
3. HAYGLASS, K. T. — Allergy: who, why and what to do about it, *Immunol. Today*, 1995, **16**, 505.
4. DEVRIES, J. E. *et al.* — Regulation of IgE synthesis by cytokines, *Curr. Opin. Immunol.*, 1991, **3**, 851.
5. SHANTI, K. N. *et al.* — Identification of tropomyosin as the major shrimp allergen and characterization of its IgE binding epitopes, *J. Immunol.*, 1993, **151**, 5354.
6. BOREL, Y. *et al.* — Food allergens transformed into tolerogens, *Int. Arch. Allergy Immunol.*, 1995, **107**, 264.

Thesis Abstract (Ph.D.)

Supramolecular chemistry: A bile acid based approach by Photon Rao
Research supervisor: Prof. Uday Maitra
Department: Organic Chemistry

1. Introduction

We have made use of the rigid, bifacial and chiral framework of bile acids in three distinct types of chemistry: 1) Among the forces of recognition the ones most studied are a) pi-stacking b) H-bonding c) electrostatic attraction and d) dispersive forces. In our studies we have used the first two for molecular recognition. 2) The chiral nature of bile acid was exploited in the asymmetric synthesis of Troger's base. 3) Novel dendritic fragments were synthesized from bile acids.

2. Results and discussion

2.1. *Bile acid-based molecular tweezer for ditopic hydrogen bonding*

The receptor **1** bearing a pair of convergent carboxyl groups was designed following molecular modeling and was synthesized in a sequence of three simple steps. Receptor **1** was found to bind 9-butyladenine and biotin methyl ester in $CDCl_3$ at 27°C with association constants of 3,500 M^{-1} and 1,700 M^{-1}, respectively.

2.2. *H-bonding in nucleobases*[1]

A carboxylic acid can bind a 9-alkyladenine derivative *via* the Watson-Crick (WC) mode or the Hoogsteen (HG) mode. 9-Butyladenine was titrated with three aromatic and three aliphatic carboxylic acids. The binding of aromatic carboxylic acids showed exclusive and in one case a predominant downfield shift of the 8-H signal whereas the binding of aliphatic carboxylic acids was accompanied by a predominant upfield shift of the 2-H. These observations were correlated with the preponderance of the HG type of complex for aromatic carboxylic acids and WC type of complexes for aliphatic carboxylic acids.

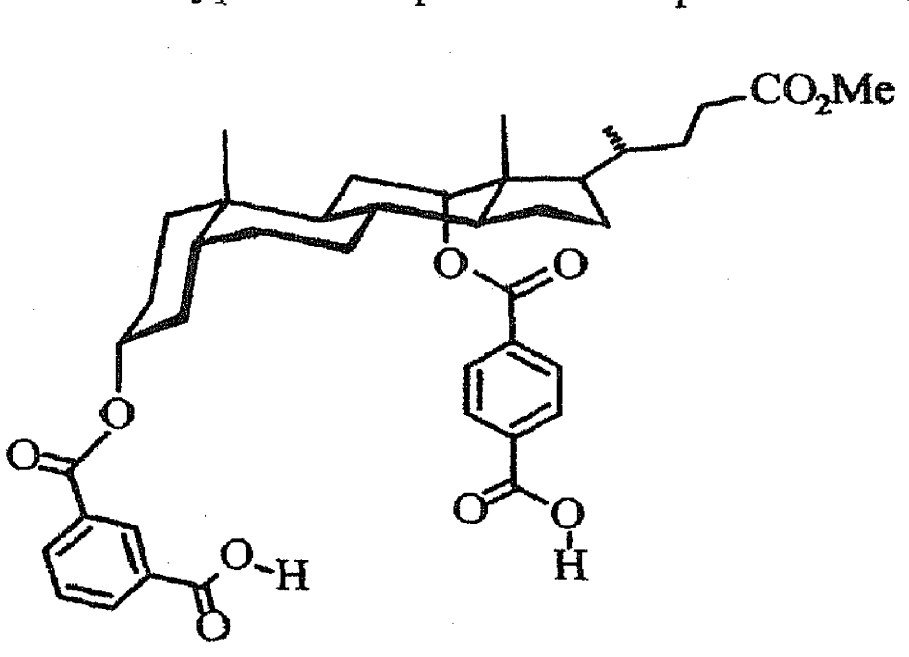

1

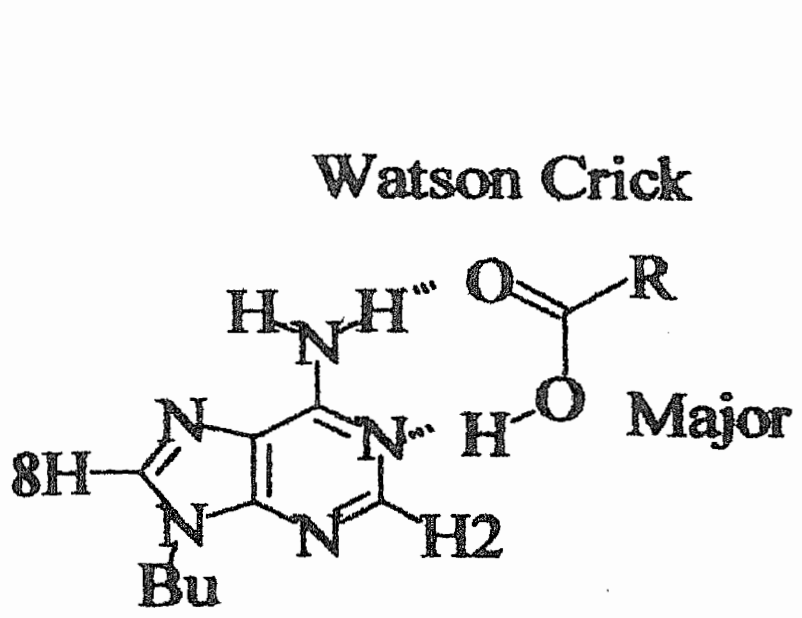

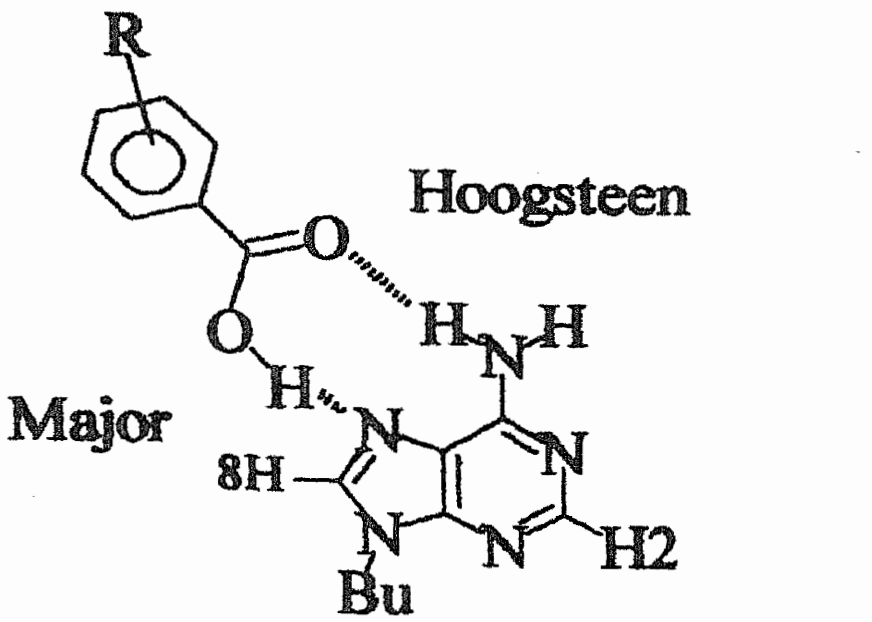

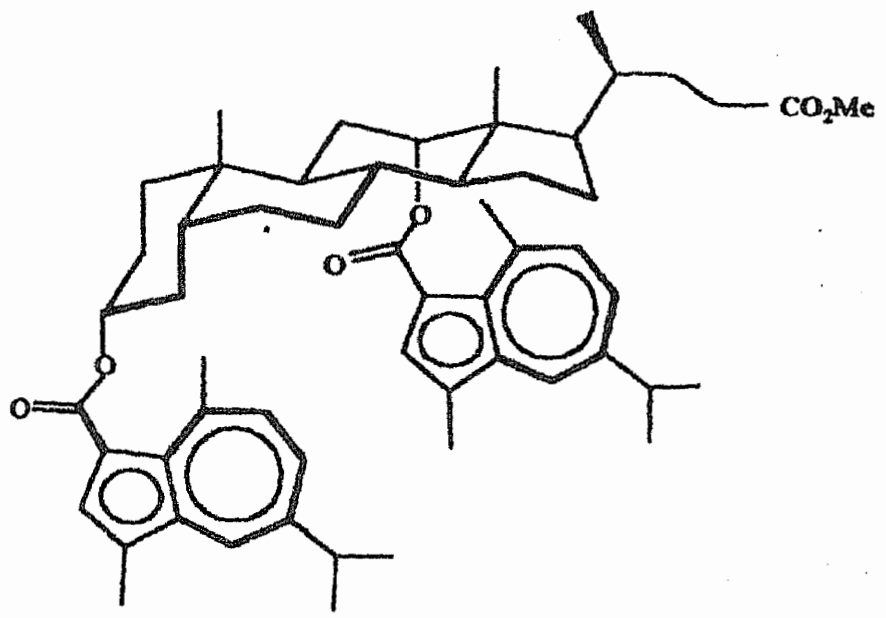

2

2.3. *Bile acid-based molecular tweezer possessing guaiazulene moieties*[2]

The first example of a synthetic receptor **2** comprising of an azulene derivative – guaiazulene, was synthesized on the methyl deoxycholate backbone. Host **2** showed K_a's of 5 M^{-1} with picric acid and 13 M^{-1} with trinitrofluorenone in $CDCl_3$ at 27°C. However, binding improved considerably in nonpolar media. Following an extraction based protocol, **2** was found to bind picric acid with a K_a of 55 M^{-1} in CCl_4 and 225 M^{-1} in cyclohexane: CCl_4 (1:1) at 26°C.

2.4. *Chemistry of Tröger's base analogues*

The effect of spacer-length on diastereoselective coupling of aniline fragments to form Tröger's base analogs (**3**, **4**, **5** and their diastereomers) was examined. Under cyclization conditions involving trifluoroacetic acid and urotropine the diastereoselection altered with changing spacers.

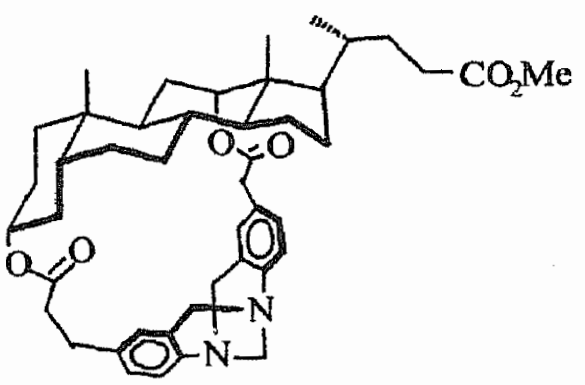

3

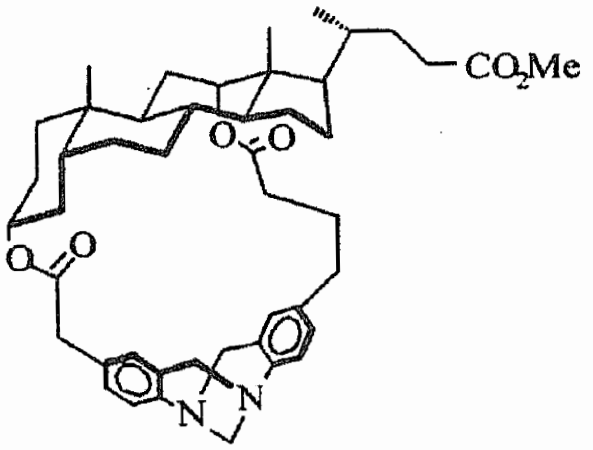

4

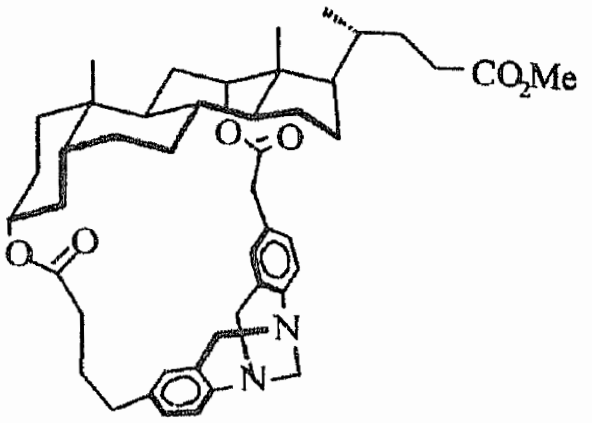

5

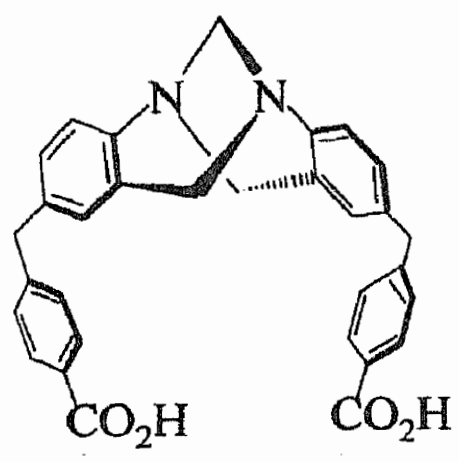

6

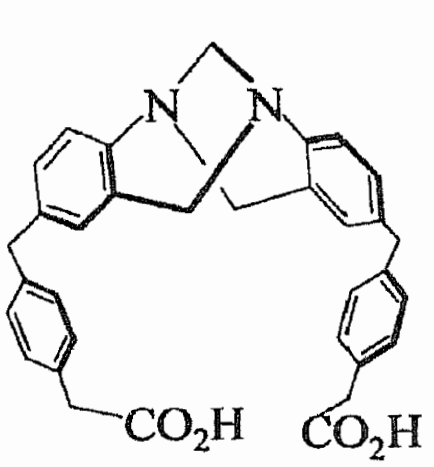

7

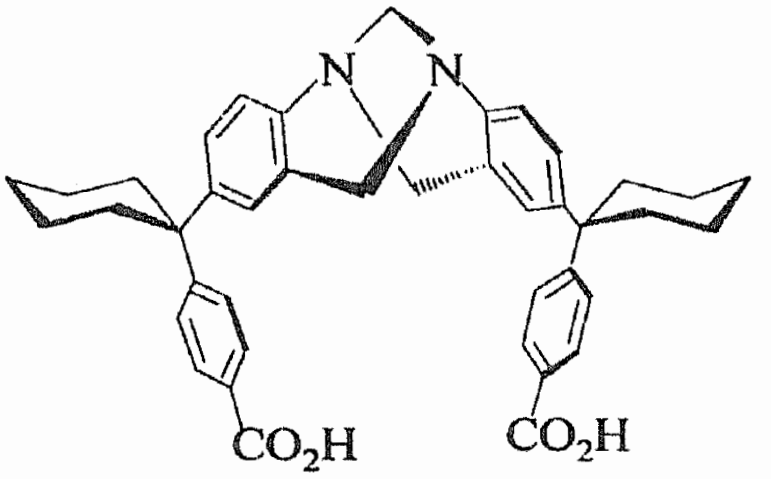

8

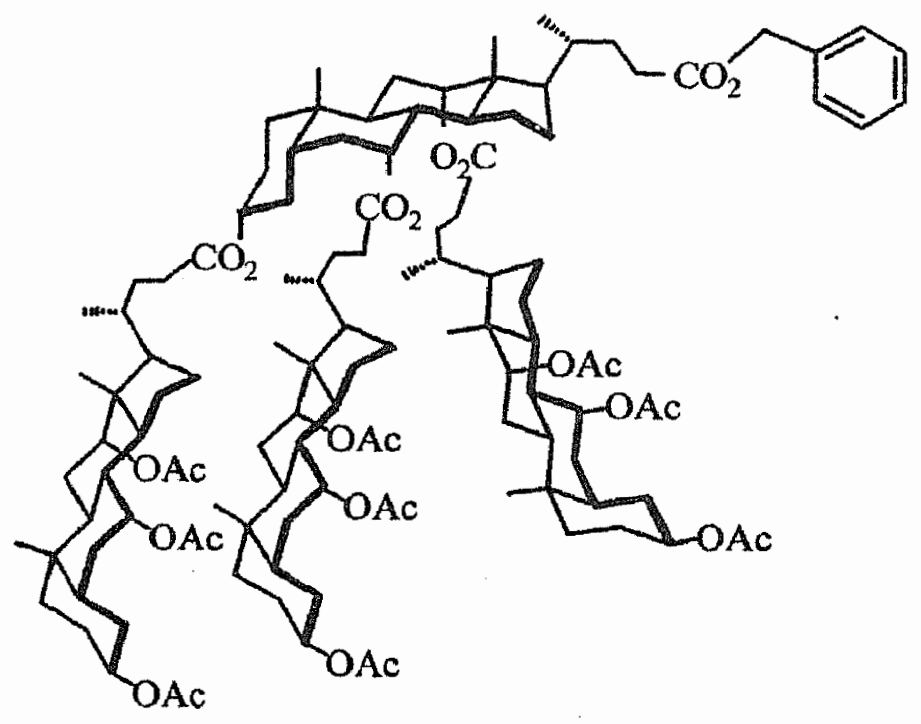

9

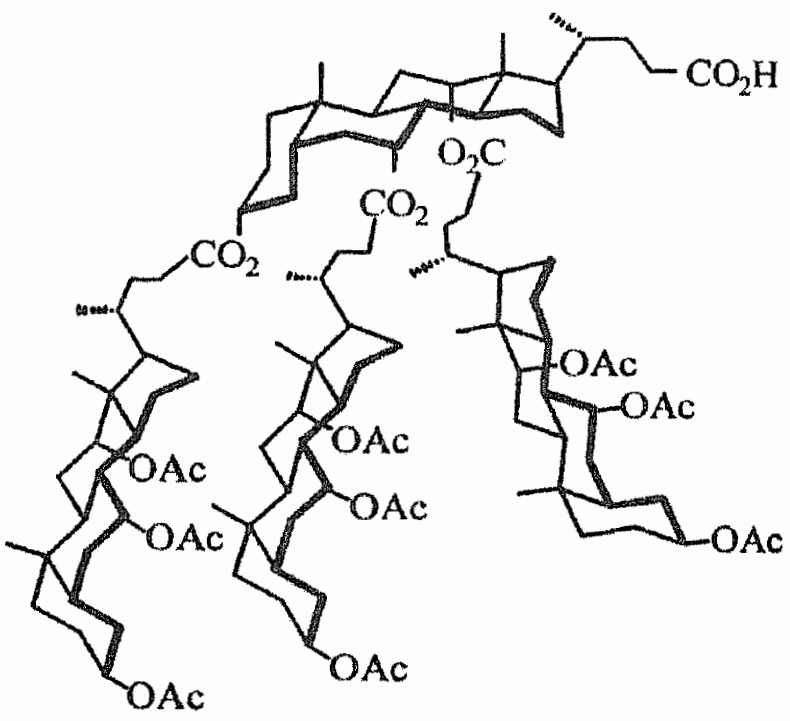

10

A new class of Tröger's base analogs **6** and **7** containing carboxyl-appended phenyl rings was synthesized. Compounds **6** and **7** were found to be almost insoluble in common organic solvents like $CHCl_3$, CH_2Cl_2, etc. However, in derivative **8** the insolubility was overcome by design.

2.5. *Bile acid-based hyperbranched molecules*[3]

In a program initiated towards the use of bile acids in the synthesis of hyperbranched molecules, *chiral* tetrameric dendrons **9** and **10** were synthesized. This is the first use of bile acids in dendritic chemistry.

References

1. LANCELOT, G. *J. Am. Chem. Soc.*, 1977, **88**, 7037.
2. ZIMMERMAN, S. C. *Topics Curr. Chem.*, 1991, **165**, 33.
3. TOMALIA, D. A. AND DURST, H. D. *Topics Curr. Chem.*, 1993, **165**, 193.
4. DICKSON, J. I. AND BAILON, J. P. *Can. Metall.*, 1981, **20**, 317.

Thesis Abstract (Ph.D.)

Planning and scheduling systems for steel casting production: A new paradigm
by G. L. Shekar
Research supervisors: Drs K. Chandra Sekhar and M. H. Balasubrahmanya
Department: Management Studies

1. Introduction

Production planning, scheduling and control of production in a foundry is often difficult owing to the complexities involved in casting production, *make-to-order* system structure, unusual practices of the casting producers, and conflicting objective of maximizing resource utilization and meeting customer service. Lack of relevant data, matching unit melt quantity with job mix while pouring, wide variations of production process yields, castings rework resulting in split batches and inability to track work-in-process are some of the unique problems that make foundry scheduling very complex.[1–6] Further, foundry has an important requirement of directly linking customer order processing with scheduling.

The scant treatment of foundry scheduling in the literature, complexities involved in mathematical modeling and an opportunity to study in depth the production scheduling practices of a steel foundry motivated us to develop the general-purpose models that give pragmatic solutions to planning and scheduling problems. The work deals with developing alternative production planning and scheduling system models for the steel foundry using heuristics approach and evaluating them on foundry performance using computer simulation.

2. System study and soft system methodology

Since the foundry system under study is highly complex with interrelated problem situation, a total viewpoint of the system is considered essential to the successful development of scheduling systems. The development of overall scenario and extraction of problem space are achieved by applying Soft System Methodology (SSM).[7] SSM has captured a 'rich picture' of the steel foundry problem situations and identified the primary tasks and issues of concern, which, in turn, identified planning and scheduling activities as the major problem areas. The problem space is further selectively narrowed down to planning and scheduling of casting stage, the major resource center in the metal casting manufacturing line. The 'root definition' as obtained by SSM recognized *capacity planning* of hot metal available in a planning horizon and *scheduling* of heats as the major production planning and scheduling (PPS) activities to be incorporated in the model.

3. Model formulation

Mathematical and heuristic methods are the solution approaches attempted for the PPS problems of the foundry under study.

3.1. *Mathematical model*

In mathematical solution approach, a small scheduling problem is formulated as a classical 0-1 integer-programming model to minimize the total number of heats in a planning period and, hence, to determine the quantity and the type of jobs that should be loaded in each heat assuming a deterministic demand. However, since the size and complexity of the present problem preempted an exact method, the work resorted to develop *heuristic algorithms* for solving casting manufacturing system.[8, 9]

3.2. *Heuristic model*

Under capacity planning, three capacity planning strategy models are developed using heuristics based on (i) allocation of capacity to customers or to their orders or to both (ii) selection of orders for each customer against the capacity allocated using priority numbers and (iii) combining (i) and (ii) mentioned above. The strategy models are called customer dominant, order dominant and mixed strategy models. Further, four planning policies are developed under the above said three strategy models.

The production scheduling component, which is the most critical issue in overall planning and scheduling of any steel foundry,[10] consists of models for (i) furnace load balancing (ii) heat generation (iii) heat scheduling and (iv) generation and location of heats lost. The load-balancing model provides a balanced flow of orders through the furnaces throughout the planning horizon. The most crucial scheduling task was to generate heats for planned orders such that there is a stepwise maximization of capacity utilization of every heat (matching unit melt quantity with a job mix). The heat-generation module achieved this challenging work. The heats are generated taking into consideration constraints like pouring line, pattern rotation per day, pattern mix in corrousal and alloy-ratio profile. Each heat consists of one or more jobs of the same or different orders having metal compatibility. Once heats are generated, the third model schedules them day-wise for the planning period. The model for the generation and location of heats lost introduces perturbance during simulation of production of castings by generating random number for both the number of heats lost and its location in the planning month.

4. Computer simulation of alternate PPS systems

The heuristic models developed separately for capacity planning and production scheduling of heats are integrated into four PPS systems. In order to validate the system models, face validation, program verification and external validation have been conducted. The models are externally validated using furnace utilization, the most important foundry performance, as a criterion. In order to evaluate these systems on a set of foundry performances (furnace utilization, pour span and lateness), a simulation experiment is designed with the heuristic models as in-

puts. Though the models relate only to the casting operation, the evaluation of the systems requires performance measures of the foundry as a whole. Therefore the simulation model also includes post-pouring operations.

Since targeted niche served was an operating steel casting producer, a computer simulation experiment was carried out across three different furnace-loading criteria (FLC) and three alloy-ratio profiles (AP). For this purpose, the models were programmed in C++ using object-oriented programming system. The individual program modules were checked and verified manually by 'black box' testing using real sample data. As C++ language has the facility for 'trace and watch', logical path coverage testing was done for each function before integrating various modules to get the complete simulation model.

Internal validation of the simulation experiment was done through the validation of generated data using chi-square test. The t-test was carried out to test the significance of difference between the means of the cumulative averages of the performance measures. The steady-state results of every casting production situation (each situation is a combination of a PPS system, an FLC, and an AP) was obtained.

5. Results and discussion

It is amply demonstrated from the results that at every casting production situation, the proposed four PPS systems performed exceptionally well in achieving 84% to 98% average furnace utilization per day. This is mainly due to the powerful search algorithm built into the system models. The present production scheduling practices in the SEPET led to only about 50% to 60% furnace utilization. The pour span ranges from 0.279 to 0.336 days per casting. The pour span results indicated that variation across three APs and PPS systems for a particular FLC is not significant. It is also observed that variations in the lateness range from 19.61 to 23.03 (absolute per cent).

While evaluating the PPS System models, first the PPS Systems were ranked against steady-state values of performance measures for a particular operating condition of FLC and AP. Then using relative weights of each performance measure (determined based on foundry experts' ranking of each performance measure through a small survey) composite ranking indices were established. It was found out from the survey that furnace utilization is the most important foundry performance as its relative weight is 0.4595 compared to pour span weight of 0.2712 and lateness weight of 0.2672. Hence, our main focus on maximum furnace utilization while developing PPS systems for the foundry is substantiated. Finally, based on the composite ranking indices the PPS systems were ranked facilitating selection of a PPS system given an operating condition.

In order to test the robustness of the systems developed, a sensitivity analysis was also performed to study the effect of changes of four important parameters under different operating conditions. The parameters were (i) AP (ii) pouring line capacity (iii) specified quota of monthly capacity, and (iv) specified outstanding load. The models were found to be robust particularly about furnace utilization. Finally, a general framework of concepts for designing PPS systems for a foundry has been developed taking inspiration from the work of Wild.[11]

6. Contribution of the work

- An important and complex PPS problem found in steel foundries but has not been dealt adequately in the literature has been addressed.
- A comprehensive PPS system models are developed using heuristic approach for solving capacity planning and production scheduling problems at the critical casting stage that is, to our knowledge, first of its kind.
- The search algorithm designed for matching unit melt quantity with job mix at the time of pouring of every heat is a very significant contribution of this research work since every heat ensures efficient furnace utilization thereby improving resource productivity. Irrespective of the PPS systems, AP and FLC, this algorithm has demonstrated its efficiency in searching and making optimal job mix.
- *Soft System Methodology* is used for the first time in foundry to capture and define highly complex and interrelated problem situation. Expression of the problem situation with a 'rich picture' is totally new in the area of foundry scheduling.
- Since little has been written about metal-casting operations planning from a policy perspective, a general framework of concepts for PPS system has been developed as an outcome of the study.
- Alternative PPS systems are developed in this study that can be applied not only to jobbing or batch-type steel foundries but also to other types of foundries.
- The effects of variations in AP and pouring line capacity on furnace utilization are also established.

7. Conclusion

It can be concluded from this work that highly complex foundry scheduling problems can be addressed by heuristic approach. The academic novelty in this study is that heuristic models are designed based on real-world foundry practices. The search algorithm has solved the crux of the problem of matching unit melt quantity with optimal job mix for every heat. The systems proposed are practically applicable.

References

1. LAW, T. D. Outline requirements for a production planning and control system for a foundry, First Report of Working Group M62 (E7)-Production Control, *Br. Foundryman*, 1983, **76**, 56–59.

2. LAW, T. D. Third Report of Working Group M62 (E7). What is production control? *Br. Foundryman*, December 1985, 509–510.

3. LAW, T. D. Fourth Report of Working Group M62 (E7). Foundry Production Control for the 80s and 90s: Functional overview and database requirements, *The Foundryman*, June 1988, 306–312.

4. LAW, T. D. Fifth Report of Working Group M62 (E7). Foundry production control for the 80s and 90s: Production planning scheduling, *The Foundryman*, March 1989, 9–13.

5. LAW, T. D. Sixth Report of Working Group M62 (E7). Foundry production control for the 80s and 90s: Production monitoring and data capture, *The Foundryman*, July 1990, 306–312.

6. LAW, T. D. Seventh Report of Working Group M62 (E7). Foundry production control for the 80s and 90s: Management information, *The Foundryman*, 1990, 363–367.

7. CHECKLAND, P. *Systems thinking, systems practice*, Wiley, 1981.

8. IGNIZIO, J. P. A brief introduction to expert systems, *Comput. Op. Res.*, 1990, **17**, 523–533.

9. PANWALKAR, S. S. AND ISKANDER, W. A survey of scheduling rules, *Op. Res.*, 1977, **25**, 45–61.

10. SOUTHALL AND LAW, T. D. Approaches to improved job scheduling in foundries, *Br. Foundryman*, 1980, **73**, 287–291.

11. WILD, R. *Operations management: A policy framework*, Pergamon, 1980.

Thesis Abstract (M.Sc. (Engng))

Some new handover schemes for mobile cellular communication systems by Shreekanth P. Lakshmeshwar
Research supervisor: D. K. Anvekar
Department: Electrical Communication Engineering

1. Introduction

The increasing demand for cellular communications access and the evolution of wireless networks towards personal communication systems (PCS) require a substantial improvement in quality of service (QoS) provided by such systems. Present cellular architectures are the basis for the future PCS. Some major topics that need further research are handover management, channel allocation, mobility management and issues related to packet data communications. Handover plays a major role in these systems by providing uninterrupted communication link irrespective of user mobility. As the demand for capacity in a cellular network is increased, smaller and smaller cells are deployed. This leads to an increase in the number of cell-boundary crossings by a mobile subscriber (MS). Forced termination of an ongoing call because of handover failure is less desirable than dropping a new call. The basic idea of handover algorithms is to give some sort of priority to handover calls over new calls, thus increasing the handover success rate at the cost of new call blocking. Keeping this in mind, the research has considered handover zone-based queuing algorithms. Two such schemes are first-come-first-serve scheme (FCFSS) and measurement-based prioritization scheme (MBPS).[1] In FCFSS, the handover requests are served on first-come first-serve basis, whereas in MBPS, the requests are served based on the received power levels from current and target base stations. Here, higher priority is given to that MS which is nearest to the target base station. Hence, MBPS performs better than FCFSS. In this research, an analysis of these schemes is carried out in a new way to study their performance. As an improvement over these schemes, a new pre-emptive queue-processing scheme has been proposed which is described later.

When existing cellular networks are also used for packet data communication, host mobility imposes making changes to several assumptions on which existing wireline systems oper-

ate. In particular, networks that include wireless links and mobile hosts suffer from delays and packet losses that are unrelated to congestion. The packet losses are severe at the time of handover when mobile host moves from one cell to the other. Also, there is a possibility of burst packet errors. A good handover algorithm is needed to reduce this effect. Keeping this in mind, the second part of this research work is focused on the investigation of a new pre-handover zone-based packet multicasting scheme, which is described later.

2. Analysis of some major handover algorithms

To validate the basic simulation process used in the research, an analytical study of FCFS and MBPS was first carried out. For this, traffic model generally used in cellular system performance analysis has been considered. With the presented model, analysis of FCFS and MBPS schemes has been carried out using a new approach. Expressions for new call blocking probability and handover failure probability have been derived. The variations of these parameters with the traffic intensity have been plotted. The results have been compared with simulation results obtained with single cell simulation model. The analytical results are consistent with simulation results, which clearly indicate the validity of the simulations.

3. Pre-emptive queue-processing scheme

A new scheme[2] for reducing of handover failures in mobile cellular communication systems is proposed. In the scheme, reassignment of priorities for handover requests enqueued in adjacent cells is carried out to release a channel for a handover request, which is about to fail. For this, two new parameters, namely, critical zone (CZ) and safety margin (SM) zone have been defined similar to handover zone as fractions of handover zone (HZ). The major algorithmic steps of this scheme are as follows:

- Whenever there is a request for a new call, if there is a free channel in the cell and there are no handover requests in the MBPS queue, then it is allowed, otherwise, it is dropped.
- Whenever a handover request arrives in a cell, if there is any free channel available it is allocated; otherwise, the request is put in MBPS queue.
- Whenever MS enters the critical zone the priority change requests are sent to the adjacent cells.
- Suppose there is a channel release in a particular cell, say first cell, because of a call completion or an MS moving out of the cell, and if this cell has a priority change request from an adjacent cell, say second cell, then first cell gives higher priority of MSs (if any in the queue) coming from the second cell. That is, first cell allocates the released channel to an MS coming from the second cell which will in turn release a channel in second cell. The channel released by such an MS in the second cell is allocated to the MS which is entering the second cell and in the critical zone and thus preventing it from being force-terminated. If there is no priority request from any of the adjacent cells, then MBPS is followed.
- If any MS in the MBPS queue has entered the safety margin zone, then its priority is not altered.

The performance evaluation of the pro7posed scheme has been carried out by simulation of 4-cell linear and 49-cell hexagonal cellular structures. For a typical critical zone length of 30% of handover zone length, the new scheme has shown reduction in handover failure probability, call in-completion probability and handover delay as compared to that of MBPS scheme at busy traffic condition. Therefore, this new scheme can be utilized in modern cellular network to achieve performance improvement. But this scheme has additional overhead of inter-base-station communication, which is required to perform pre-emptive queue processing. However, with the modern high-speed wireline and optical networks this communication overhead is easily manageable.

4. PHZ-based packet multicasting scheme

The packet multicasting schemes such as simple buffering scheme, delayed buffering scheme and subgroup buffering scheme have been proposed in technical literature.[3] But these schemes incur a certain level of buffer overhead in the BSs. This may be a drawback when buffer size in BSs is limited and when many MHs try to use the cellular data services. Keeping this in view, to reduce the buffer overhead in the BSs, a new pre-handover zone handover scheme has been proposed in this research. Major features of the new scheme are as follows:

- A pre-handover zone (PHZ) is defined similar to a handover zone (HZ), based on the received power levels from current BS and target BS. This is the zone in which MH moves before entering the handover zone.
- Whenever an MH is in PHZ or HZ, the packets are multicasted to both the base stations adjacent to PHZ or HZ. But, the packets are received by MH from current BS only.
- As the MH is handed over to the target BS, it just receives the next packets which are buffered there.
- There is no intervention of MTSO at the time of handover, but it is involved only at the time of MH's entry into and departure from the multicasting zone.
- The length of the PHZ can be set depending on the reception of power levels and the system buffer capacity.

The new scheme is advantageous as it minimizes: 1) loss of packets as compared to non-multicasting schemes, 2) the buffer overhead as compared to other multicasting schemes, and 3) handover delay.

The performance evaluation of these schemes is carried out through a simulation of linear cells in a highway model with an MH traveling in these cells. The results have shown reduction in buffer overhead. Performance improvement in terms of other parameters such as packet missing probability, waiting time, and buffer length have been studied for different values of PHZ length, packet size, handover delay and packet arrival rate. These results are compared with those for the delayed buffering scheme. The results have shown better performance of the PHZ based scheme over the delayed buffering scheme.

5. Conclusion

In this research, two new handover schemes have been proposed for mobile cellular communication. Performance evaluation of both the above schemes has been carried out through simulation by using appropriate traffic and system models. It has been shown that the

lation by using appropriate traffic and system models. It has been shown that the performance of both the schemes is superior as compared to the existing schemes. Thus, the research work has made significant contributions in terms of development of two new schemes for handovers which can be easily implemented in the modern cellular communication networks as also in the future packet data cellular systems such as UMTS (Universal Mobile Telephone System).

References

1. TEKINAY, S. AND JABBARI, B. A measurement based prioritization scheme for handovers in mobile cellular networks. *IEEE J. Select Area Commun.*, 1992, **10**, 1343–1350.

2. LAKSHMESHWAR, S. P. AND ANVEKAR, D. K. Pre-emptive queue processing scheme for handovers in mobile cellular communication systems. *IEEE Conf. on Personal Wireless Communication*, 1997, Mumbai, pp. 28–32.

3. HA, E., CHOI, Y. AND KIM, C. A new pre-handoff scheme for picocellular networks. *IEEE Conf. on Personal Wireless Communication*, 1996, pp. 140–143.

Thesis Abstract

Wideband microstrip antennas for mobile communications by S. Shanthi
Research supervisor: T. S. Vedavathy
Department: Electrical Communication Engineering

1. Introduction

Mobile communication[1] is receiving greater attention currently and since it is wireless in nature, issues related to propagation and antenna become important. Small antennas are preferred to mount on the handset or the mobile. Most suitable for this type of applications are the mi-

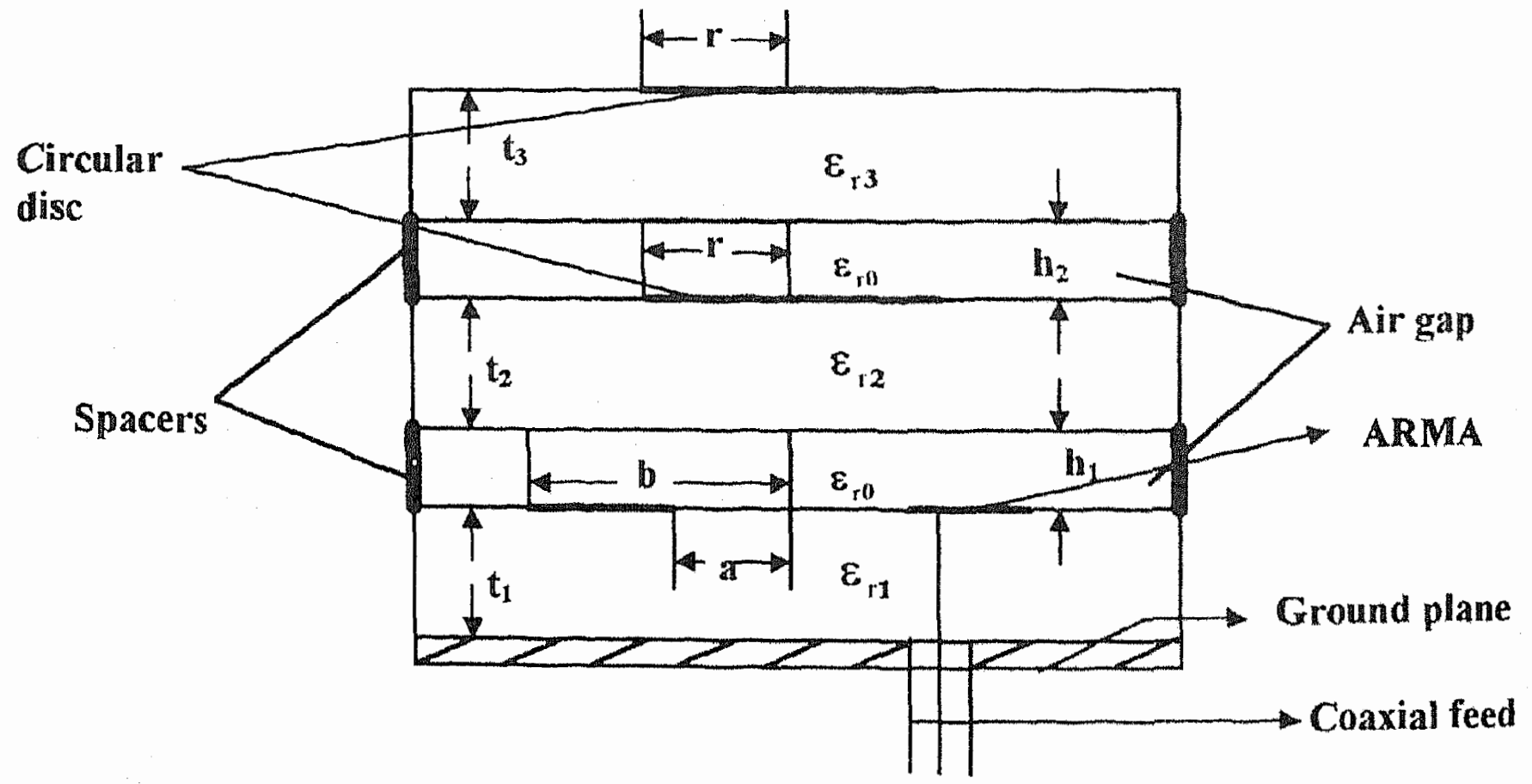

FIG. 1. Three-layer stacked MSA.

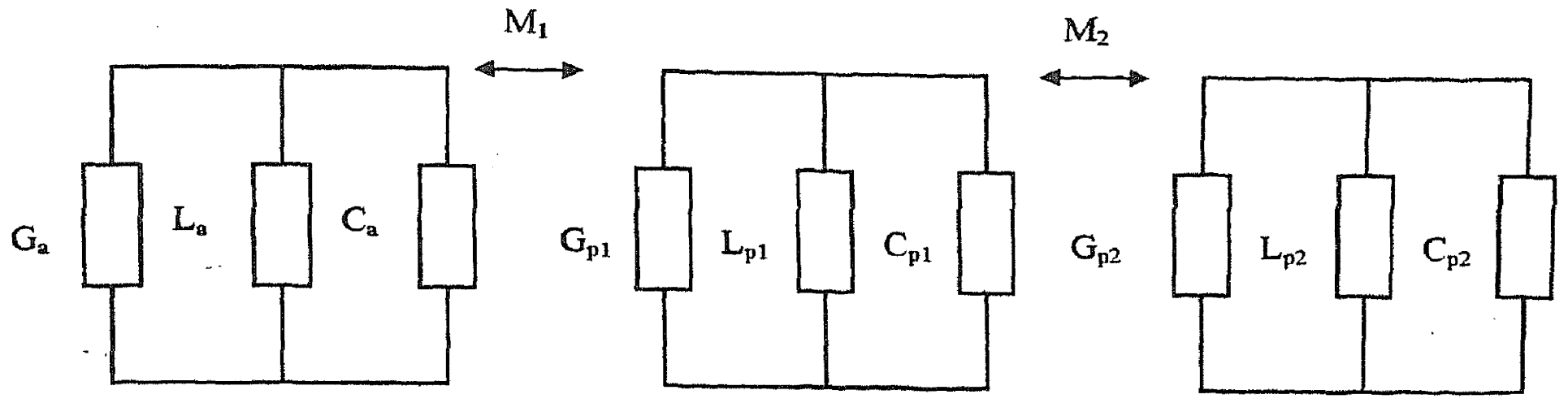

FIG. 2. Equivalent circuit of three-layered stacked MSA.

crostrip antennas (MSAs). While such antennas have all the attractive characteristics, they have two drawbacks, namely, narrow bandwidth and low power handling capacity. Power handling is a problem of the substrate breakdown potential and no solution seems to exist till such materials become available. However, the problem of bandwidth can be solved to a great extent by methods of stacking and addition of parasitic patches around the active patch and also log-periodic arrangement of the elements in an array of MSAs.

2. Three-layer stacked MSA

It is observed that by stacking the radiating patch and a passive parasite, an improvement in the bandwidth to the extent of 10–15% is obtained and a 20–25% increase obtained by adding two passive parasites or in the three-layered stacked structure.

In this structure, two circular patches are placed above an annular ring MSA (ARMA), where the ARMA is excited in the TM_{21} mode and circular discs are parasitically excited in the TM_{11} mode as shown in Fig. 1. The Modal Expansion technique is used to carry out the analysis of this stacked configuration, where the field components are written in terms of the mode vectors. The input impedance calculated from the *modal expansion model* is expressed as a GLC resonator.

It is found that the percentage bandwidth is directly proportional to the coupling coefficients of the parasitic patches (Table I). The percentage bandwidth obtained is higher only when the resonant frequency of the driven patch and parasitic patches are identical. Frequency response and variation of resistance of the patch are studied as a function of distance from the centre to the periphery to locate a 50Ω point for the feed probe.

Table I
Variation in percentage bandwidth with the coupling coefficients of the upper and lower patches for a three-layered stacked structure

*k*1	*k*2	% Bandwidth
0.1	0.1	10
0.1	0.2	14.1421
0.1	0.3	17.3205
0.2	0.1	14.1421
0.2	0.2	20
0.2	0.3	24.4949

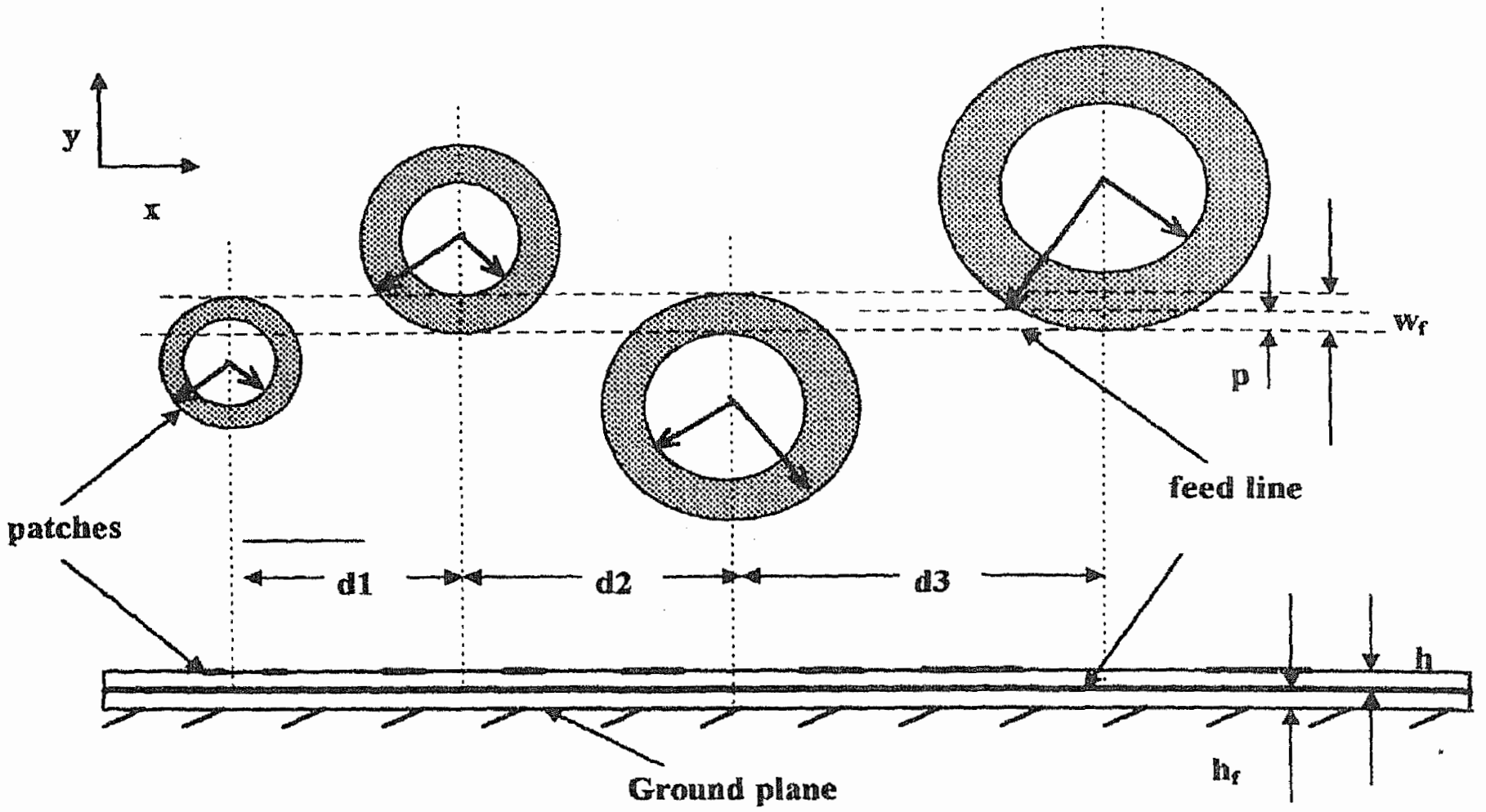

FIG. 3. Configuration of LPA of ARMAs and its cross-section.

It is found from the analysis that with one parasitic disc above the ARMA the percentage bandwidth is found to be 10 for a $k_1 = 0.1$ and with a second parasitic patch, increases to 14 for a $k_2 = 0.2$.

It is observed from the frequency response that the bandwidth is found to increase by stacking and with increase in the substrate thickness. At the resonant frequency of the stacked structure, a return loss of approximately 10 dB is observed.

3. Log periodic array of MSAs

The design follows the well-known principle of log periodic scaling of arrays (LPA). Two structures, namely, LPA of ARMAs and LPA of concentric ARMAs are analysed in the following section.

Table II

Design parameters of LPA of ARMAs for $\tau = 1.05$ and $\varepsilon_r = 2.55$ assuming uniform thickness $h = 1.6$ mm, $h_f = 1.6$ mm and $w_f = 1.035$ cm. (a & b are the inner and outer radius of the ARMA and d is the interelement distance)

m	A (cm)	b (cm)	d (cm)	% bandwidth per patch	F_r (GHz)
1	0.4	0.8	1.84	2.982	12.6635
2	0.42	0.84	1.932	2.141	11.2564
3	0.442	0.884	2.029	1.649	10.0804
4	0.46305	0.9261	–	1.340	9.08386

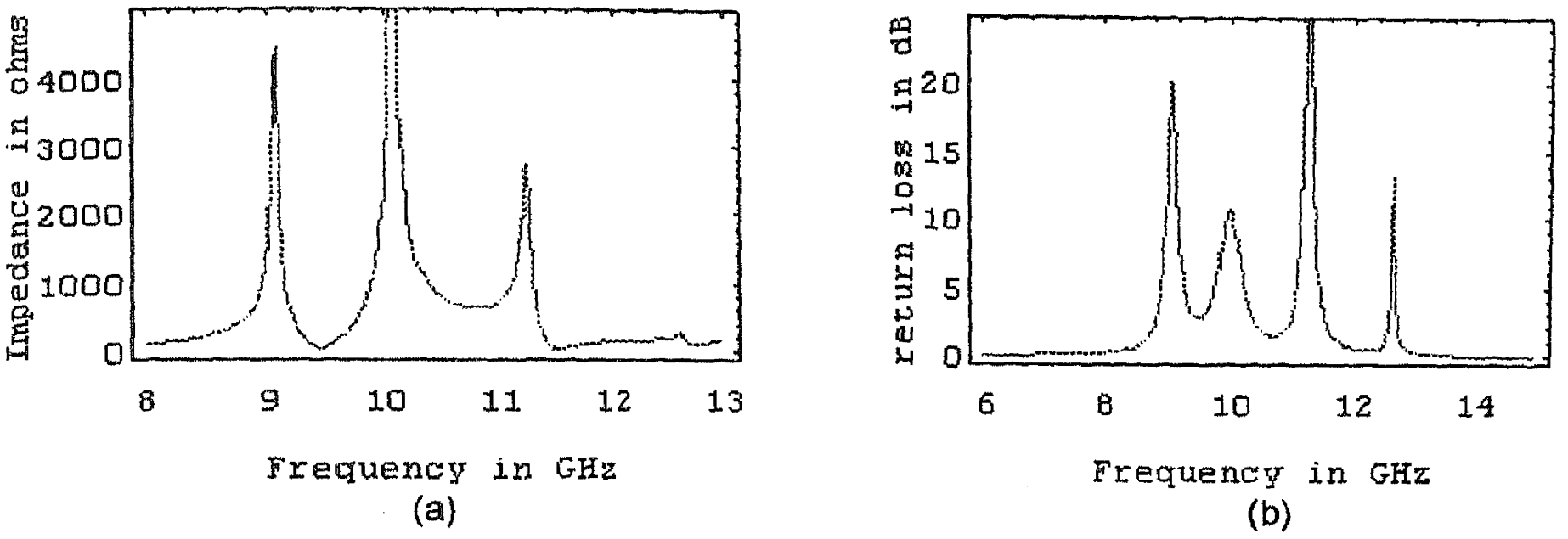

FIG. 4. (a) Impedance response and (b) return loss of four elements of LPA of ARMAs.

3.1. *EM-coupled LPA of ARMAs*

Figure 3 shows the LPA of electromagnetically coupled four ARMAs designed over a frequency band from 4.37 to 5.06 GHz. The scale factor is chosen to be 1.05. This structure is analysed using the *modal expansion model.*

In this design, average bandwidth of the patch is 2.028% for an LPA of four elements of ARMA. Since the number of elements chosen in the LPA is 4, the maximum bandwidth obtained is 8.1%. However, higher percentage of bandwidth can be obtained by increasing the number of elements and decreasing τ.

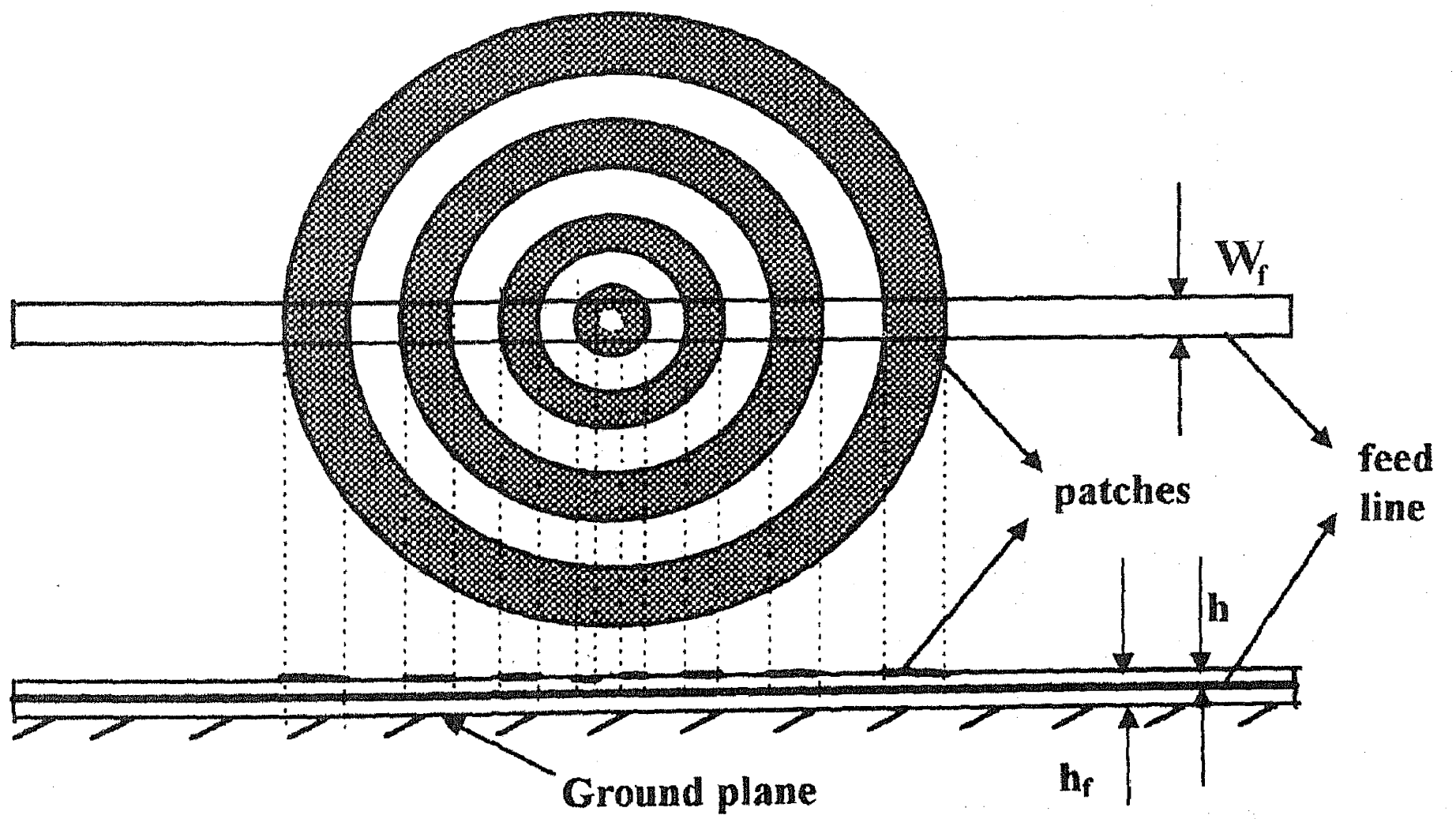

FIG. 5. Configuration of concentric ARMA arranged in the LP fashion (Ref. Table 3 for dimensions).

Table III
Design parameters of the elements of LPA of ARMA for $\tau = 1.05$ and $\varepsilon_r = 2.55$ assuming uniform thickness $h = 1.6$ mm, $h_f = 1.6$ mm and $w_f = 1.035$ cm. (a & b are the inner and outer radius of the ARMA and d is the interelement distance)

m	a (cm)	b (cm)	D (cm)	% bandwidth per patch	F_r (GHz)
1	2	2.4	0.48	18.1788	8.07417
2	2.88	3.456	0.6912	12.0888	5.38278
3	4.1472	4.97664	0.995328	8.08808	3.63701
4	5.97197	7.16636	–	5.46857	2.47917

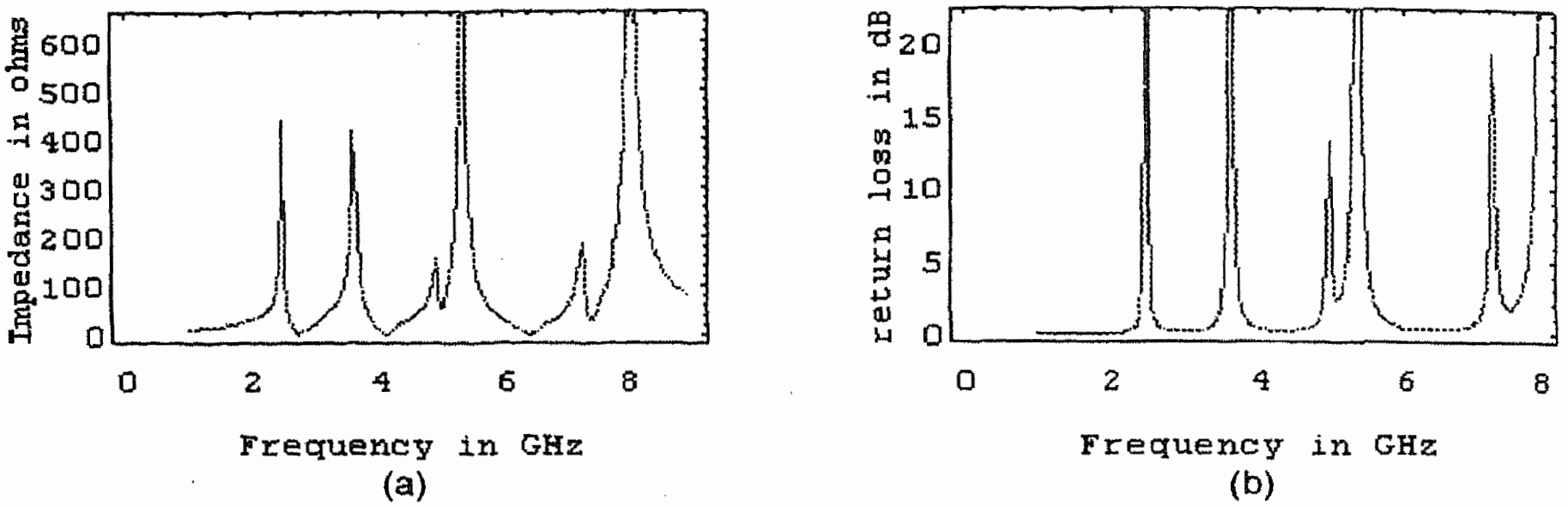

FIG. 6. Impedance response and return loss of 4 elements of LPA of concentric ARMA.

3.2. *EM-coupled LPA of concentric ARMAs*

In this design, the average bandwidth of the patch is 10.9561% for a log-periodic array of four elements of concentric ARMA with $\tau = 1.2$ and $\varepsilon_r = 2.55$ and since the number of elements chosen in the log-periodic array is 4, the maximum bandwidth obtained is 43.8243%.

Reference

1. *IEEE Trans. Antennas Propagation*, Special Issue, Jan. 1981, Vol.

Thesis Abstract (M.Sc.(Engng))

The applications of artificial neural network (ANN) in SF_6 breakdown studies in non-uniform field gaps by Sandeep Chowdhury
Research supervisor: Prof. M. S. Naidu
Department: High Voltage Engineering

1. Introduction

Sulphur hexafluoride (SF_6), a strongly electronegative gas is being increasingly used as an insulating medium in electrical power equipments such as switchgears, transformers and cables for its well-known advantages like high dielectric strength, good arc quenching ability, etc.

In SF_6-filled electrical equipment, where the electric field distribution is kept rather uniform, very good dielectric performances are obtained in reduced volumes. However, in practice, the electric field in the gas gap is distorted by field non-uniformities created by metallic particles present in the gas and surface protrusions on the electrodes, which produces local stress enhancements.

For this reason, the inhomogeneous field breakdown in SF_6 has been extensively studied by various researchers in order to get more information on the physical processes that influence the breakdown mechanisms. In many of these studies the inhomogeneous field distribution has been simulated by rod-plane gaps, where the field nonuniformity is varied by varying either the rod diameter or the gap spacing. The breakdown characteristics (corona inception and breakdown voltage characteristics) of compressed SF_6 have been reported under varying conditions of gas pressures, rod diameters, gap spacings and applied voltage waveforms (DC, AC and impulse).

In the absence of any mathematical model describing a relationship between the experimental parameters (gas pressure, rod diameter, and gap spacing) and the corresponding breakdown voltages for a particular voltage waveform, an attempt has been made in the present work to apply an artificial neural network (ANN) to obtain such a correlation.

The Projection Pursuit Learning Network (PPLN) has been used as the ANN model. Breakdown data for four different voltage waveforms were used to train the network—DC (positive and negative polarity), AC, Standard LI (+1.2/50 μs) and Standard SI (+250/2500 μs).

The ANN was first trained with these data so as to obtain a smooth regression surface interpolating the training data. The regression surface thus obtained was thereafter used to generate the breakdown and corona inception voltages within the range of gas pressures and field non-uniformities studied, where no data is available.

2. The ANN model

Figure 1 shows the architecture of the Projection Pursuit Learning (PPL) network[1–3] used in the present study.

The PPLN is a two-layer feedforward learning network whose trainable parameters are:

1. The hidden layer weights denoted by $\{\alpha_{kj}, j = 1,\ldots, n\}$, connecting all the input units to the kth hidden neuron.
2. The unknown (trainable) 'smooth' activation functions denoted by $\{f_k, k = 1,\ldots, m\}$ of the kth hidden neuron, which are hermite functions defined as

$$f_k(z_k) = \sum_{r=1}^{R} c_{kr} h_r(z_k) \tag{1}$$

where the c_{kr}s are the coefficients of the hermite functions h_rs, and R is called the *order* of the hermite function f_k, which is a constant set by the user.

The hermite functions are orthonormal and defined by

$$h_r(z_k) = (r!)^{-1/2}\pi^{1/4}2^{-(r-1)/2}H_r(z_k)\phi(z_k) \tag{2}$$

where $H_r(z_k)$s are the hermite polynomials constructed in a recursive manner as

$$H_0(z_k) = 1 \tag{3}$$

$$H_1(z_k) = 2z_k \tag{4}$$

$$H_r(z_k) = 2[z_k H_{r-1}(z_k) - (r-1)H_{r-2}(z_k)] \tag{5}$$

$r = 2, 3, 4,\ldots$

and $\phi(z_k)$ is the weighting function

$$\phi(z_k) = \frac{1}{\sqrt{2\pi}} e^{-z_k^2/2} \tag{6}$$

3. The output layer weights denoted by β_k connecting the kth hidden neuron to the output unit

The output of the network is mathematically expressed as

$$\hat{y}_l = \sum_{k=1}^{m} \beta_k f_k \left(\sum_{j=1}^{n} \alpha_{kj} x_{jl} \right) \tag{7}$$

where $\hat{y}_l$ is the actual output of the network computed by the ANN for the lth training pattern.

The training of all the weight parameters, β_k, $\{c_{kr}\}$ and $\{\alpha_{kj}\}$, is based on the criteria of minimizing the MSE (mean-squared-error), or the so-called L_2 loss function defined as

$$L_2 = \sum_{l=1}^{p} [y_l - \hat{y}_l]^2 \tag{8}$$

$$= \sum_{l=1}^{p} \left[y_l - \sum_{k=1}^{m} \beta_k f_k \left(\alpha_k^T \mathbf{x}_l \right) \right]^2 \tag{9}$$

which is the sum-squared error between the desired and the actual output over all the training patterns.

The characteristic features of the training process of the PPL network are as follows:

1. The network is built gradually, starting from a single hidden neuron; additional hidden units and weights are added subsequently during the training process till a minimum architecture is obtained which gives a satisfactory solution for the given problem.
2. Instead of training the whole network after a new hidden unit is added, the PPL algorithm first trains only the new hidden unit. After the new hidden unit is trained, the parameters associated with the previously installed hidden units are updated one

unit at a time. Thus the PPL network is trained in a neuron-by-neuron manner and not as a whole entity.

3. Further simplification is obtained by training a single hidden unit in a layer-by-layer manner. For this purpose, the parameters that have to be trained after adding the kth hidden unit are divided into three groups (α_k, $\mathbf{c}_k$ and β_k). Each group is updated separately for that particular neuron.

3. Results and discussion

For DC applied voltages (both polarities), the breakdown data[4] consisted of both the corona inception and breakdown voltage characteristics of rod–plane gaps. The field nonuniformity was varied by varying the rod diameter values in the range 1.0 to 6.3 mm for a fixed gap spacing of 20 mm. The gas pressure was varied in the range 1 to 5 bar. The breakdown voltage data were trained in the corona-stabilised region while the corona onset data were trained separately in the full pressure range. The ANN had 2 inputs, one corresponding to the pressure values, and the other to the rod diameter values. The maximum training error for both polarities was around 5% of the desired output value.

Similar breakdown data[5] for AC applied voltage had a pressure range of 1 to 6 bar and rod diameter range of 1 to 10 mm for a fixed gap spacing of 60 mm. The maximum training error was 5% of the desired output value.

For impulse voltage waveforms (standard LI (1.2/50 μs) and SI (250/2500 μs)), the breakdown data consisted of breakdown voltage values only. In this case, the field nonuniformity was varied by varying separately two experimental parameters – the rod diameter as well as the gap spacing. The ANN had 3 inputs, corresponding to pressure values, rod diameter values and gap spacing values. The training data for both types of impulse waveforms had pressure range of 1 to 5 bar, rod diameter range of 1 to 12 mm and gap spacing range of 10 to 100 mm. The maximum training error for both waveforms was around 10% of the desired output value.

The generalization of the network for all the applied voltage waveforms showed fairly good consistency with the general nature of the breakdown voltage characteristics reported in the literature. For DC and AC waveforms, the corona inception characteristics were linear while the breakdown voltage characteristics were nonlinear and exhibited corona stabilization effect. The corona stabilization effect was more pronounced with an increase in the field nonuniformity. Negative polarity DC had lower corona inception voltages but its breakdown voltage characteristics exhibited a more pronounced corona stabilization effect compared to the positive polarity waveforms. The SI breakdown characteristics were similar to those of AC and DC waveforms while for LI breakdown characteristics, the corona stabilization effect was prominent only for higher field nonuniformities.

4. Conclusions

ANN may be used in gas breakdown studies for handling multidimensional nonlinear regression tasks with accuracy within tolerable limits. This may considerably reduce the time and expense of undertaking lengthy experimental processes for generating necessary data.

References

1. HWANG, J. N., LAY, S. R., MAECHLER, M., MARTIN, R. D. AND SCIMERT, J. — Regression modeling in back-propagation and projection pursuit learning, *IEEE Trans. Neural Networks*, 1994, 5, 342–353.

2. HWANG, J. N., YOU, S. S., LAY, S. R. AND JOU, I. C. — The cascade correlation learning: a projection pursuit learning perspective, *IEEE Trans. Neural Networks*, 1996, 7, 272–289.

3. KWOK, T. Y. AND YEUNG, D. Y. — Use of bias term in projection pursuit learning improves approximation and convergence properties, *IEEE Trans. Neural Networks*, 1996, 7, 1168–1183.

4. MALIK, N. H. AND QURESHI, A. H. — The influence of voltage polarity and field nonuniformity on the breakdown behaviour of rod–plane gaps filled with SF_6, *IEEE Trans. Electl Insulation*, 1979, **EI-14**, 327–333.

5. ZWICKY, M. — Breakdown phenomenon in SF_6 and very inhomogeneous large rod–plane gaps under 50-Hz AC and positive impulse voltages, *IEEE Trans. Electl Insulation*, 1987, **EI-22**, 317–324.

6. MANJUNATH, B. S. — *Inhomogeneous electric field breakdown in pure SF_6 gas under AC and impulse voltages*, M.Sc. (Engng) thesis, Deptt. of High Voltage Engineering, Indian Institute of Science, May 1991.